# Control of Gαq signaling dynamics and GPCR cross-talk by GRKs

Xiang, Guoqing; Acosta-Ruiz, Amanda; Radoux-Mergault, Arthur; Kristt, Melanie; Kim, Jihye; Moon, Jared D.; Broichhagen, Johannes; Inoue, Asuka; Lee, Francis S.; Stoeber, Miriam Carolin; Dittman, Jeremy S.; Levitz, Joshua

**How to cite**

XIANG, Guoqing et al. Control of Gαq signaling dynamics and GPCR cross-talk by GRKs. In: Science advances, 2022, vol. 8, n° 47, p. eabq3363. doi: 10.1126/sciadv.abq3363

This publication URL: https://archive-ouverte.unige.ch/unige:165354
Publication DOI: 10.1126/sciadv.abq3363

SIGNAL TRANSDUCTION

# Control of $G\alpha_q$ signaling dynamics and GPCR cross-talk by GRKs

**Guoqing Xiang[1,2]†, Amanda Acosta-Ruiz[1]†, Arthur Radoux-Mergault[3], Melanie Kristt[1], Jihye Kim[2], Jared D. Moon[1], Johannes Broichhagen[4], Asuka Inoue[5], Francis S. Lee[2], Miriam Stoeber[3], Jeremy S. Dittman[1], Joshua Levitz[1,2]***



**Numerous processes contribute to the regulation of G protein–coupled receptors (GPCRs), but relatively little is known about rapid mechanisms that control signaling on the seconds time scale or regulate cross-talk between receptors. Here, we reveal that the ability of some GPCR kinases (GRKs) to bind $G\alpha_q$ both drives acute signaling desensitization and regulates functional interactions between GPCRs. GRK2/3-mediated acute desensitization occurs within seconds, is rapidly reversible, and can occur upon local, subcellular activation. This rapid desensitization is kinase independent, insensitive to pharmacological inhibition, and generalizable across receptor families and effectors. We also find that the ability of GRK2 to bind G proteins also enables it to regulate the extent and timing of $G\alpha_q$-dependent signaling cross-talk between GPCRs. Last, we find that G protein/GRK2 interactions enable a novel form of GPCR trafficking cross-talk. Together, this work reveals potent forms of $G\alpha_q$-dependent GPCR regulation with wide-ranging pharmacological and physiological implications.**

## INTRODUCTION

G protein–coupled receptors (GPCRs) respond to a wide array of extracellular signals to initiate diverse intracellular signaling pathways via heterotrimeric G proteins. The temporal dynamics of intracellular signaling, including the activation and deactivation kinetics of the response to brief, extended, or repeated exposures, are critical determinants of the biological effects of GPCR activation (*1*). For example, recently developed fluorescent sensors for neurotransmitters and neuromodulators have shown phasic patterns of brief, seconds-long extracellular release events in vivo that reflect the temporal profile of physiological receptor signaling (*2*–*4*). In contrast, activation of GPCRs with drugs, such as opioids, can lead to signaling over hours or days that can elicit compensatory processes such as tolerance (*5*). Furthermore, many different GPCRs are coexpressed within the same cell (*6*–*8*), raising the possibility that GPCRs cross-talk with each other in synergistic or antagonistic ways. For example, $G\alpha_{i/o}$-coupled receptors can produce cytosolic $Ca^{2+}$ elevations that are dependent on simultaneous activation of a $G\alpha_q$-coupled GPCR via synergistic binding of Gβγ and $G\alpha_q$ to the common effector, phospholipase C-β (PLC-β) (*9*, *10*). Together, this complexity motivates a more complete understanding of general and receptor-specific mechanisms of GPCR regulation in the context of a single GPCR subtype and cross-talk between GPCRs.

Extensive work has been done to decipher the mechanisms of GPCR desensitization, although the focus has been on slower processes that evolve over minutes or hours (*11*, *12*). GPCR kinases (GRKs) and beta-arrestins (β-arrs) mediate homologous desensitization of many GPCRs via phosphorylation and clathrin-mediated internalization, which typically happens on the tens of minutes time scale (*13*, *14*). For the most part, β-arr–dependent mechanisms are receptor specific: The propensity for desensitization is dependent on the receptor's ability to directly interact with GRKs and β-arrs. For a given receptor, this can also be ligand specific as some "arrestin-biased" agonists or modulators can preferentially promote β-arr–dependent internalization (*15*, *16*), while other "G protein–biased" agonists can elude internalization (*17*, *18*).

Compared to trafficking-dependent mechanisms, less is known about GPCR desensitization over briefer time scales (<60 s), but receptor-specific and nonspecific mechanisms have been observed. Regulator of G protein signaling (RGS) proteins can control the temporal dynamics of GPCR signaling by promoting guanosine 5′-triphosphate (GTP) hydrolysis with specificity at the level of G protein subtypes (*19*), although GPCR-specific RGS mechanisms also exist (*20*). Potassium channel tetramerization domain 12 (KCTD12) mediates desensitization of γ-aminobutyric acid type A ($GABA_B$) receptor ($GABA_BR$) signaling on the seconds time scale via its ability to bind both the $GABA_{B2}$ C-terminal tail and Gβγ proteins (*21*, *22*). At high expression levels, KCTD12 is also capable of nonspecific desensitization of other $G\alpha_{i/o}$-coupled GPCRs (*23*), suggesting that receptor nonspecific modes may also be physiological.

Rapid desensitization has also been shown to occur via GRK2 in the context of $G\alpha_{i/o}$-coupled receptors and Gβγ-dependent gating of G protein–coupled inward rectifier potassium (GIRK) channels. Raveh *et al.* (*24*) found that GIRK currents elicited by the A1 adenosine receptor or the mu-opioid receptor (MOR), but not metabotropic glutamate receptor 2 (mGluR2) or the M4 muscarinic acetylcholine receptor, can be desensitized on the <5-s time scale by GRK2 in a kinase-independent but Gβγ binding–dependent way. Similarly, we recently showed that mGluR3, but not mGluR2, can be rapidly desensitized by GRK2 in a manner that is dependent on Gβγ binding and an intact kinase domain, likely via specific interactions with the mGluR3 C-terminal tail (*25*). Fluorescence imaging studies have shown that rapid GRK2 recruitment can be directly to the activated receptor and/or to activated G proteins, depending on the receptor subtype and ligand (*26*, *27*). Together, this indicates

[1]Department of Biochemistry, Weill Cornell Medicine, New York, NY, USA. [2]Department of Psychiatry, Weill Cornell Medicine, New York, NY, USA. [3]Department of Cell Physiology and Metabolism, University of Geneva, Geneva, Switzerland. [4]Leibniz-Forschungsinstitut für Molekulare Pharmakologie, Berlin, Germany. [5]Graduate School of Pharmaceutical Sciences, Tohoku University, Sendai, Japan.
*Corresponding author. Email: jtl2003@med.cornell.edu
†These authors contributed equally to this work.

that complexity exists in the mode of GRK2 recruitment by GPCRs, which may shape the extent, timing, and receptor specificity of effects on downstream signaling.

Despite clear biochemical and structural evidence that GRK2 and GRK3 can bind to $G\alpha_q$ (*28*–*31*), the functional consequences of this interaction (*28*, *32*–*41*), particularly in terms of temporal signaling dynamics and GPCR cross-talk, are not well understood. We recently showed that the $G\alpha_q$-coupled mGluRs, mGluR1 and mGluR5, are insensitive to GRK and β-arr–mediated internalization, but their intracellular $Ca^{2+}$ responses to glutamate can be rapidly desensitized by GRK2 (*25*). Here, we show that GRK2 or GRK3, but not GRK5 or GRK6, can markedly reshape the dynamics of signaling by mGluR1 and mGluR5, to produce briefer and more repeatable release of intracellular $Ca^{2+}$ stores in response to a range of ligands and subcellularly targeted photoactivation. Mechanistic analysis reveals a general mode of kinase-independent desensitization that is dependent on $G\alpha_q$-GRK2 binding, which can sequester activated G proteins from their effectors, such as PLC-β. This mechanism is not receptor specific, as demonstrated with heterologously expressed serotonin [serotonin 2A receptor (5-$HT_{2A}$R)]–gated, acetylcholine (muscarinic acetylcholine receptor type 3 ($M_3$R)]–gated, and endogenous adenosine 5′-triphosphate (ATP) [P2Y receptor ($P_{2Y}$R)]–gated $G\alpha_q$-coupled GPCRs, and is insensitive to the widely used GRK2/3 kinase inhibitor compound 101. Furthermore, we find that $G\alpha_{i/o}$-coupled GPCRs can produce $G\alpha_q$-dependent $Ca^{2+}$ responses that are strongly desensitized by GRK2/3 binding to both $G\alpha_q$ and Gβγ. Last, we find that $G\alpha_q$/GRK2 interaction contributes to internalization of $G\alpha_q$-coupled GPCRs and can drive receptor cross-talk at the level of internalization such that coactivation of $G\alpha_q$-coupled mGluR1 enhances internalization of the $G\alpha_{i/o}$-coupled MOR or mGluR3. Together, this study shows not only that GRKs play a central role in phosphorylation-dependent internalization, but also that they are also regulators of $G\alpha_q$ signaling dynamics and GPCR cross-talk.

## RESULTS

### GRK2 and GRK3, but not GRK5 or GRK6, reshape $Ca^{2+}$ signaling dynamics following group I mGluR activation

The precise timing of $Ca^{2+}$ signaling is a central aspect of many cellular processes, and $G\alpha_q$-coupled receptors are one of the primary drivers of intracellular $Ca^{2+}$ release via activation of PLC-β and subsequent gating of inositol 1,4,5-trisphosphate ($IP_3$) receptors (*42*, *43*). Motivated by our recent findings (*25*), we asked which GRKs can alter the intracellular $Ca^{2+}$ response to activation of mGluR1 or mGluR5, the group I subfamily of mGluRs. These mGluR subtypes are widely expressed $G\alpha_q$-coupled family C GPCRs that are enriched in neuronal dendrites where they control $Ca^{2+}$-dependent processes, including synaptic plasticity (*44*). Despite a high degree of sequence homology and functional overlap, each receptor produces distinct $Ca^{2+}$ responses, providing two distinct systems for testing the effects of GRKs. mGluR1 activation typically leads to slowly desensitizing transients, while mGluR5 can produce rapid protein kinase C–mediated oscillatory responses (*45*, *46*). When coexpressed in human embryonic kidney (HEK) 293T cells with the red fluorescent $Ca^{2+}$ indicator red fluorescent genetically encoded $Ca^{2+}$ indicators for optical imaging (R-GECO) (*47*), mGluR1 produced $Ca^{2+}$ responses to saturating glutamate that lasted the entire 3-min application period but showed partial desensitization that led to a full width at half maximum (FWHM) value of 40 to 70 s (Fig. 1A and fig. S1A). This desensitization is likely mediated in part by GPCR-independent $Ca^{2+}$ store regulation (*42*), as well as potential contributions from endogenous RGS proteins or GRKs.

Coexpression of GRK2 or GRK3, but not GRK5 or GRK6, led to $Ca^{2+}$ responses of similar amplitude to control conditions but with FWHM reduced to 10 to 20 s and complete desensitization back to baseline $Ca^{2+}$ levels within 30 s (Fig. 1, A and B, and fig. S1B), without altering mGluR1 surface expression (fig. S1C). Single exponential fits of the desensitization kinetics revealed a threefold decrease in $\tau_{desensitization}$ (fig. S1D), indicative of accelerated desensitization. The initial rise time in response to glutamate was also decreased from ~15 to ~5 s upon coexpression of GRK2 or GRK3 (Fig. 1, C and D). Since these experiments were performed with relatively slow perfusion speeds (exchange time ~ 5 s; see Materials and Methods), we used a fast perfusion system (exchange time ~ 0.5 s) to confirm the effects of GRK2 on the initial response to glutamate. We found very similar effects of GRK2 on both FWHM and rise time (fig. S1, E to G). We also analyzed mGluR1 $Ca^{2+}$ responses to a range of glutamate concentrations and found that across all doses, GRK2 accelerated both the desensitization and activation kinetics (fig. S1, H and I).

In response to glutamate, the initial $Ca^{2+}$ transient produced by mGluR5 was briefer than for mGluR1 but was similarly sensitive to GRK2 or GRK3, but not GRK5 or GRK6 (Fig. 1, E and F). GRK coexpression also had no effect on mGluR5 surface expression (fig. S1J). The rise time of mGluR5 responses was also accelerated by GRK2 or GRK3 (fig. S1, K and L). Unlike mGluR1, mGluR5 showed oscillatory responses over the course of the 3-min glutamate application (Fig. 1G). GRK2 or GRK3 coexpression decreased the proportion of cells that showed oscillatory responses, with the majority showing a single transient (Fig. 1H). Thus, GRK2 and GRK3 can both shape the initial kinetics of mGluR5 responses and control the duration of oscillatory signaling.

We further characterized the effects of GRK2 on group I mGluR $Ca^{2+}$ signaling by asking if accelerated signaling kinetics were dependent on the ligand type. Application of the widely used orthosteric group I mGluR agonist (S)-3,5-Dihydroxyphenylglycine (DHPG) produced mGluR1 $Ca^{2+}$ responses that were similarly altered by GRK2 coexpression (fig. S2, A to C). In addition, coapplication of the mGluR1 positive allosteric modulator (PAM) Ro 67-7476 (*48*) did not alter the sensitivity of glutamate responses to GRK2 coexpression (fig. S2, D to F). Last, we applied the mGluR5-specific agonistic PAM ("ago-PAM") VU0360172 (VU036) (*49*) and observed a similar GRK2-induced acceleration of desensitization and ON kinetics (fig. S2, G to I) and a reduction in the proportion of cells showing oscillations (fig. S2, J and K). Together, these data show that GRK2 can reshape the $Ca^{2+}$ signaling dynamics of group I mGluRs without any apparent ligand specificity.

To assess the dependence of these effects on GRK2/3 expression levels, we first titrated the amount of transfected GRK2 while maintaining a constant amount of mGluR1 (see Materials and Methods). We found that as we increased the amount of GRK2–green fluorescent protein (GFP) complementary DNA (cDNA) transfected, we observed both an increase in fluorescence intensity (fig. S3A) and a decrease in the FWHM and rise time of glutamate responses (fig. S3, B to D). The effect of GRK2-GFP cotransfection on response kinetics saturated at levels beyond 0.5 μg per well (used for all experiments unless otherwise stated) but was clearly seen with as little as 0.01 μg per well. It is worth noting that we observed a drop in transfection

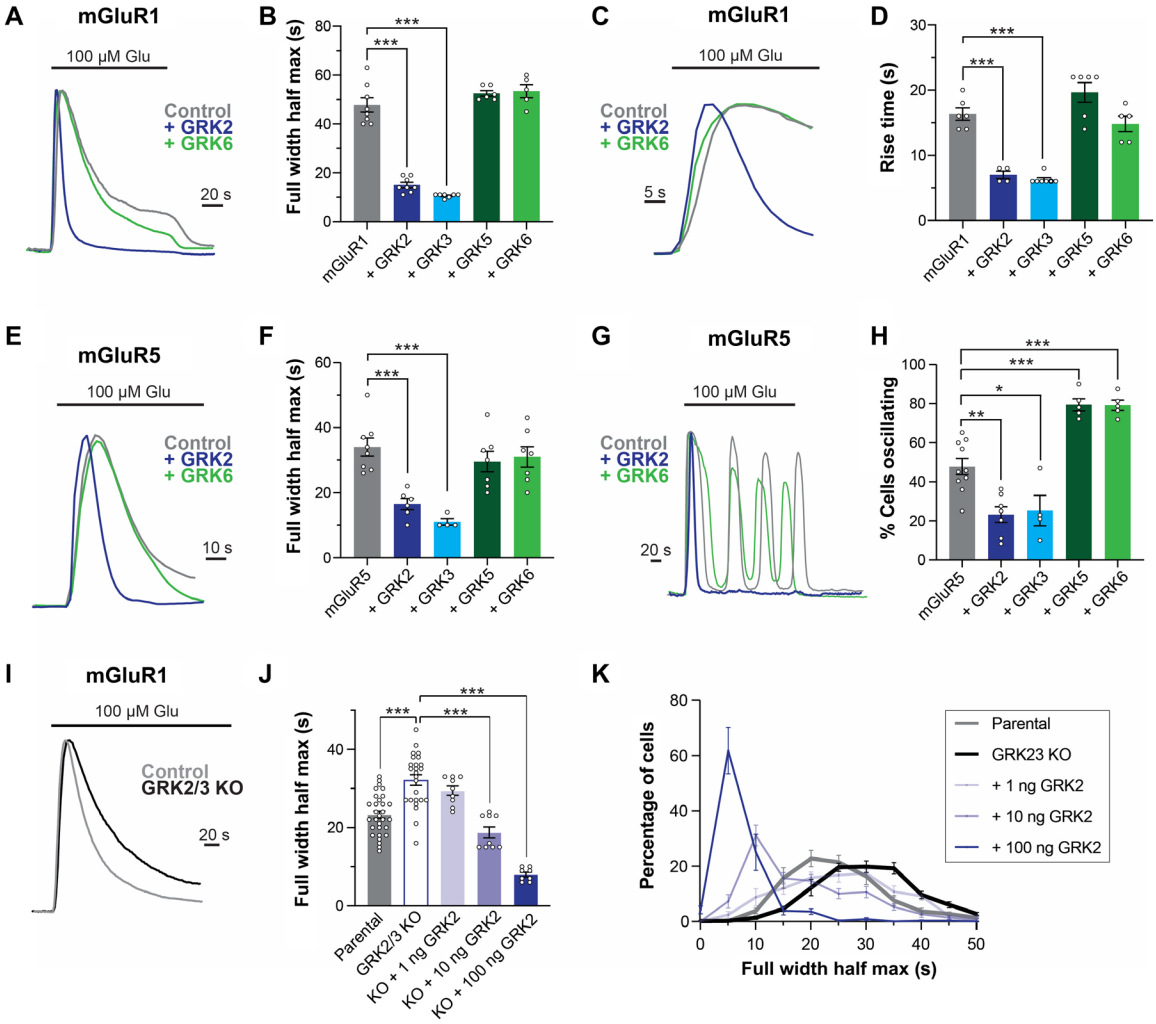


**Fig. 1. GRK2 and GRK3, but not GRK5 or GRK6, rapidly desensitize group I mGluR-mediated $Ca^{2+}$ responses.** (**A**) Representative normalized average traces showing kinetics of glutamate-induced R-GECO response to mGluR1 activation. (**B**) Summary bar graph showing effects of GRK coexpression on FWHM. (**C**) Zoom-in to representative traces showing the effect of GRK2 on ON kinetics of R-GECO response. (**D**) Summary bar graph showing the effects of GRK coexpression on rise time. (**E** and **F**) Same as (A) and (B), but for mGluR5. (**G**) Representative individual cell traces showing oscillatory responses, which are reduced with GRK2 coexpression. (**H**) Summary bar graph showing the effects of GRKs on the proportion of cells showing oscillatory responses to glutamate. (**I**) Representative normalized average traces showing kinetics of glutamate-induced R-GECO response to mGluR1 activation in parental versus GRK2/3 double KO cells. (**J**) Summary bar graph showing the effects of GRK2/3 double KO and GRK2 rescue on FWHM. (**K**) Summary histogram showing the distribution of FWHM values across individual cells for each condition and replicate in (J). Fifty to 80 cells per experiment are used to produce a normalized histogram that is averaged across separate experiments to produce mean histograms with error bars. GRK2/3 KO produces a shift in the distribution toward higher FWHM values, while GRK2 rescue produces dose-dependent shifts toward lower values and a narrower distribution. In bar graphs, each point represents an independent measurement; all graphs come from two to five separate experimental days, and error bars represent SEM. One-way ANOVA with Tukey's multiple comparisons tests. *$P < 0.05$, **$P < 0.01$, and ***$P < 0.001$.

efficiency with <0.01 μg per well GRK2-GFP DNA, which may partially explain the lack of clear effect at the lowest concentration. Next, to assess whether endogenous levels of GRK2/3 can control the $Ca^{2+}$ response dynamics, we performed experiments in recently reported GRK2/3 double knockout (KO) HEK293 cells (*50*). Compared to parental cells, GRK2/3 double KO cells showed mGluR1-driven glutamate responses with larger FWHM (Fig. 1, I and J), rise time (fig. S3, E and F), and $\tau_{desensitization}$ (fig. S3G). To rescue the effect of endogenous GRK2/3 deletion, we transfected GRK2 DNA into GRK2/3 KO cells and found a dose-dependent decrease in FWHM (Fig. 1J), rise time (fig. S3F), and $\tau_{desensitization}$ (fig. S3G) but no alterations in the proportion of cells responding to glutamate (fig. S3H). Single-cell analysis revealed a similar shift in the mean FWHM due to GRK2/3 double KO and rescue, as shown in histograms in Fig. 1K where high doses of GRK2 DNA (≥10 ng) produced narrower FWHM distributions. We also tested mGluR5 responses and found that GRK2/3 KO cells showed a higher proportion of cells showing glutamate-induced $Ca^{2+}$ oscillations (fig. S3I) but a similar overall percentage of cells responding to glutamate (fig. S3J). Together, these data show that different GRK2/3 expression levels can control $G\alpha_q$-driven $Ca^{2+}$ signaling kinetics in a graded manner and that endogenous GRK2/3 levels are sufficient to elicit clear regulation.

To determine whether the effects of GRK2 on mGluR1/5 $Ca^{2+}$ signaling kinetics are due directly to changes in $Ca^{2+}$ release from

the endoplasmic reticulum (ER) versus changes in cytosolic $Ca^{2+}$ handling, we performed a similar experiment using the ER-targeted calcium indicator "ER-GCaMP6" (*51*). Upon glutamate application, a clear decrease in fluorescence was observed in cells expressing mGluR1 (Fig. 2A). Coexpression of GRK2 markedly decreased the FWHM (Fig. 2B) and rise time (Fig. 2C), as was seen with cytosolic $Ca^{2+}$ responses (Fig. 1). As we previously reported (*52*), mGluR5 ER-GCaMP6 responses were oscillatory on a similar time scale to cytosolic responses (Fig. 2D). GRK2 coexpression had a similar effect on mGluR5 desensitization kinetics (Fig. 2E) and the proportion of cells showing oscillatory responses (Fig. 2F). Together, these data show that GRK2 can reshape the timing of $Ca^{2+}$ release from the ER in response to mGluR1 or mGluR5 activation.

Canonical GRK-mediated desensitization depends on receptor phosphorylation and internalization that leads to either receptor degradation or recycling (*14*). The former leads to a long-lasting down-regulation of ligand responses, while the latter leads to an extended refractory period (~15 to 60 min) where diminished responses will occur before surface receptor levels are restored. We asked whether GRK2-mediated desensitization of mGluR1 $Ca^{2+}$ responses is reversible, enabling a rapid recovery on the ~5-min time scale, or would lead to a longer-lasting inhibition. We applied a recovery-from-desensitization protocol where a full 3-min glutamate application was followed by a variable recovery period of 1 to 6 min before reapplication of glutamate. Notably, GRK2 coexpression did not preclude recovery and even accelerated the recovery of $Ca^{2+}$ signal

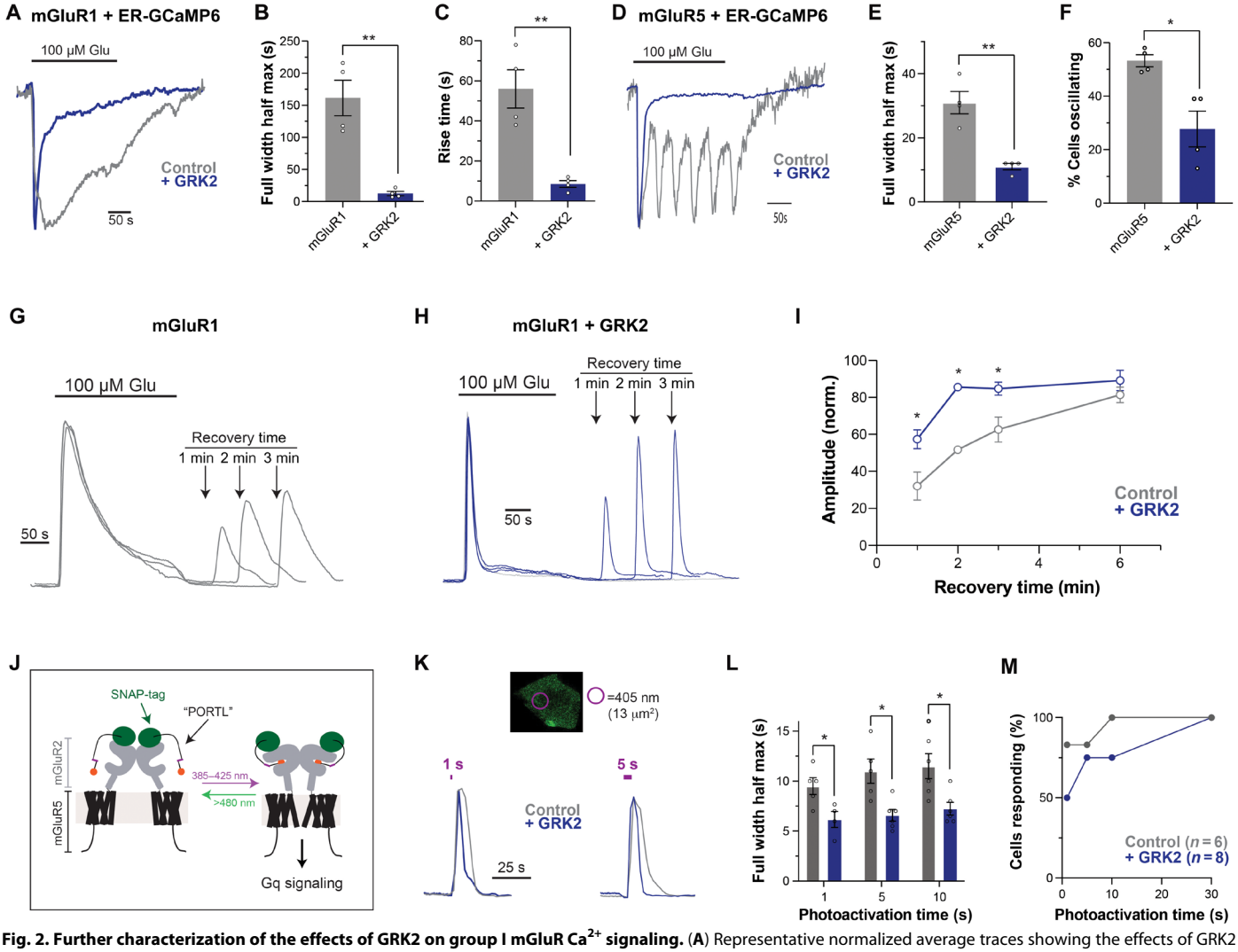


**Fig. 2. Further characterization of the effects of GRK2 on group I mGluR $Ca^{2+}$ signaling.** (**A**) Representative normalized average traces showing the effects of GRK2 coexpression on ER-GCaMP6f response to mGluR1 activation. (**B** and **C**) Summary bar graph showing the effects of GRK coexpression on FWHM (B) and rise time (C). (**D**) Representative normalized single-cell traces showing the effects of GRK2 coexpression on ER-GCaMP6f response to mGluR activation. (**E** and **F**) Summary bar graph showing the effects of GRK2 coexpression on FWHM (E) and the proportion of cells with oscillations (F). (**G** and **H**) Representative normalized average traces showing recovery from desensitization after variable time windows for control (G) and GRK2 coexpression (H). (**I**) Summary graph showing faster recovery with GRK2 coexpression. (**J**) Schematic showing SNAP-mGluR2-mGluR5 chimera and "BGAG" PORTLs for optical agonism of mGluR5 signaling. (**K**) Representative image showing photoactivation area (purple circle) and representative normalized single-cell traces showing the whole-cell GCaMP6f response to brief photoactivation. (**L**) Summary bar graph showing FWHM in response to photoactivation for different durations. (**M**) Summary graph showing increases in responsiveness in the absence of GRK2. Each point represents an independent measurement; all graphs come from two to three separate experimental days, and error bars represent SEM. For (B), (C), (E), (F), and (L): unpaired *t* test; for (L): two-way ANOVA with Tukey's multiple comparisons test. $^*P < 0.05$ and $^{**}P < 0.01$.

amplitude compared to control conditions (Fig. 2, G to I). This shows that rapid GRK2-mediated desensitization is reversible, consistent with a trafficking-independent mechanism. The accelerated recovery observed may be a consequence of the rapid desensitization of $Ca^{2+}$ release that leads to less store depletion and enables a more complete recovery of baseline $Ca^{2+}$ gradients compared to control conditions.

While GRK2 can clearly reshape the $Ca^{2+}$ response to global agonist application on the tens of seconds to minutes time scale, many GPCRs can be activated for briefer periods with agonist localization confined to subcellular areas. For example, mGluR5 may be activated following bursts of synaptic firing that can lead to extrasynaptic glutamate elevations that are as brief as 1 to 5 s (*53*, *54*). To stimulate mGluR5 with spatiotemporal precision, we used our recently reported photopharmacological approach that uses a "PORTL" (photoswitchable, orthogonal, remotely tethered ligand) termed benzylguanine-azobenzene-glutamate ($BGAG_{12,400}$) to photoactivate a chimeric SNAP-tagged mGluR2-mGluR5 construct containing the entire signaling transmembrane and regulatory C-terminal domains of mGluR5 (Fig. 2J) (*52*, *55*). We coexpressed SNAP-mGluR2-mGluR5 with GCaMP6f in HEK293T cells and stimulated a 13-$\mu m^2$ area with 405-nm light for 1, 5, 10, or 30 s, which produced $Ca^{2+}$ transients with an FWHM of 10 to 15 s (Fig. 2K). Coexpression of GRK2 decreased the FWHM of these responses across all photoactivation times (Fig. 2L), showing that GRK2 can also shape response kinetics within this spatiotemporally confined regime. Notably, GRK2 coexpression also decreased the proportion of cells showing responses to 1- or 5-s stimuli (Fig. 2M), suggesting that GRK2 may also serve as a barrier to increase the threshold stimulation required for a cellular response.

### Mechanistic analysis of GRK2/3-mediated desensitization of $G\alpha_q$-mediated signaling

Given the rapid onset and reversibility of GRK2 effects on mGluR1 and mGluR5 $Ca^{2+}$ responses, we hypothesized that kinase-independent G protein binding underlies GRK2 regulation. Multiple crystal structures of bovine GRK2 bound to Gβγ have been solved (*56*–*62*), and one structure revealed simultaneous binding to Gβγ and $G\alpha_q$ via the GRK2 pleckstrin homology and RGS homology (RH) domains, respectively (*31*) (Fig. 3A).

We introduced mutations known to disrupt either Gβγ (R587Q) (*63*) or $G\alpha_q$ (D110A) binding (*34*) and tested the ability of GRK2 to regulate group I mGluR $Ca^{2+}$ responses. We also tested a "kinase-dead" (K220R) mutation that prevents the enzymatic kinase activity of GRK2 (*64*). Consistent with our prior study (*25*), GRK2-K220R produced the same effects on FWHM and rise time as wild-type GRK2 (Fig. 3, B to E, and fig. S4, A and B). In contrast, GRK2-D110A coexpression did not alter $Ca^{2+}$ signaling kinetics. GRK2-R587Q showed wild type–like effects (Fig. 3, B to E, and fig. S4, A and B), with the exceptions of small decreases in the extent of FWHM reduction for mGluR1 (Fig. 3C) and both percent cells oscillating and rise time for mGluR5 (fig. S4, B and C), which were not significantly different from wild-type GRK2. GRK2 mutants showed comparable expression to wild-type GRK2 (fig. S4D). Upon treatment with a lower glutamate concentration (10 μM), GRK2-R587Q produced only a partial desensitization of mGluR1 responses compared to wild-type GRK2 (fig. S4, E to G), indicating that Gβγ binding can be a secondary contributor to rapid desensitization. Mutation to the $G\alpha_q$ binding site (D110A) also abolished the desensitizing effects of GRK3, indicating that this is a general mechanism within the GRK2/3 subfamily (fig. S4, H to J). These results clearly demonstrate that GRK2/3-mediated rapid regulation of group I mGluR $Ca^{2+}$ responses are kinase independent but dependent on $G\alpha_q$ interaction. Given this kinase independence, we asked whether the effects of GRK2 would be sensitive to the widely used GRK2 kinase inhibitor compound 101 ("cmpd101"). We compared crystal structures of GRK2 with and without cmpd101 bound (*57*) and observed no clear global conformational changes or local structural alterations at the $G\alpha_q$ interface (fig. S4K). Consistent with this, application of 30 μM cmpd101 had no effect on the ability of GRK2 to rapidly desensitize mGluR1-mediated glutamate responses (Fig. 3, F and G), although it fully blocked agonist-induced internalization of the MOR as a positive control (fig. S4L).

We also asked whether phospholipid interaction is necessary for GRK2-mediated desensitization of $Ca^{2+}$ responses. We produced the double mutation K567E/R578E (Fig. 3A), which has been reported to impair anionic phospholipid binding to reduce GRK2-mediated GPCR phosphorylation and internalization (*63*) and abolish rapid desensitization of GIRK channel activation by $G_{i/o}$-coupled GPCRs (*24*). The K567E/R578E double mutation did not alter the ability of GRK2 to accelerate desensitization of mGluR1-induced $Ca^{2+}$ responses (Fig. 3, H and I), suggesting a major role for phospholipid interaction in GRK2/Gβγ, but not GRK2/$G\alpha_q$, binding. Consistent with GRK2-R587Q data (fig. S4, E to G), responses to low-dose glutamate were weakly sensitive to the K567E/R587E double mutation (fig. S4, M and N).

Together, these data suggest a mechanism where GRK2 or GRK3 binds $G\alpha_q$-GTP at the plasma membrane to sequester it from the effector, PLC-β (Fig. 4A). Consistent with this competitive binding mechanism, crystal structures of $G\alpha_q$-GRK2 (*31*) and $G\alpha_q$–PLC-β3 (*65*, *66*) have shown that the binding site for each partner involves a nonidentical but highly overlapping surface on $G\alpha_q$ (Fig. 4B). Since we have previously shown that internalization of mGluR1 and mGluR5 is modest and GRK2 independent (*25*), we hypothesized that group I mGluR activation can rapidly recruit GRK2/3 to the plasma membrane primarily via G proteins rather than through direct receptor interaction. To test this, we used total internal reflection fluorescence (TIRF) microscopy to quantify the fluorescence increase associated with GRK2-GFP recruitment to the plasma membrane, as we have done previously with kappa opioid receptors (*27*). mGluR1 activation with 1 mM glutamate led to a rapid, pronounced increase in GRK2-GFP fluorescence, indicative of membrane recruitment on the same time scale as functional desensitization (Fig. 4C). To test whether this recruitment occurs via G proteins rather than direct receptor interaction, we applied the $G\alpha_q$ blocker YM-254890 and observed a near-complete loss of glutamate-induced GRK2 relocalization (Fig. 4, C and D). As a control, recruitment of GRK2-GFP by the $G\alpha_{i/o}$-coupled MOR was insensitive to YM-254890 (fig. S5, A, B). We also tested GRK2 mutants and found that, while GRK2-D110A-GFP showed wild type–like glutamate-induced membrane recruitment, a clear impairment was found for GRK2-R587Q, which was further reduced in a D110A/R587Q double mutant (fig. S5, C and D). These data are consistent with the effect of YM-254890 (Fig. 4, C and D), together arguing that GRK2-mediated desensitization of mGluR1 $Ca^{2+}$ signaling is mediated primarily by receptor-independent G protein/GRK interaction.

We next asked whether the simple competitive binding model (Fig. 4A) is sufficient to describe our data. We first reasoned that a three-state model, containing inactive ($G_0$), active ($G_1$), and desensitized

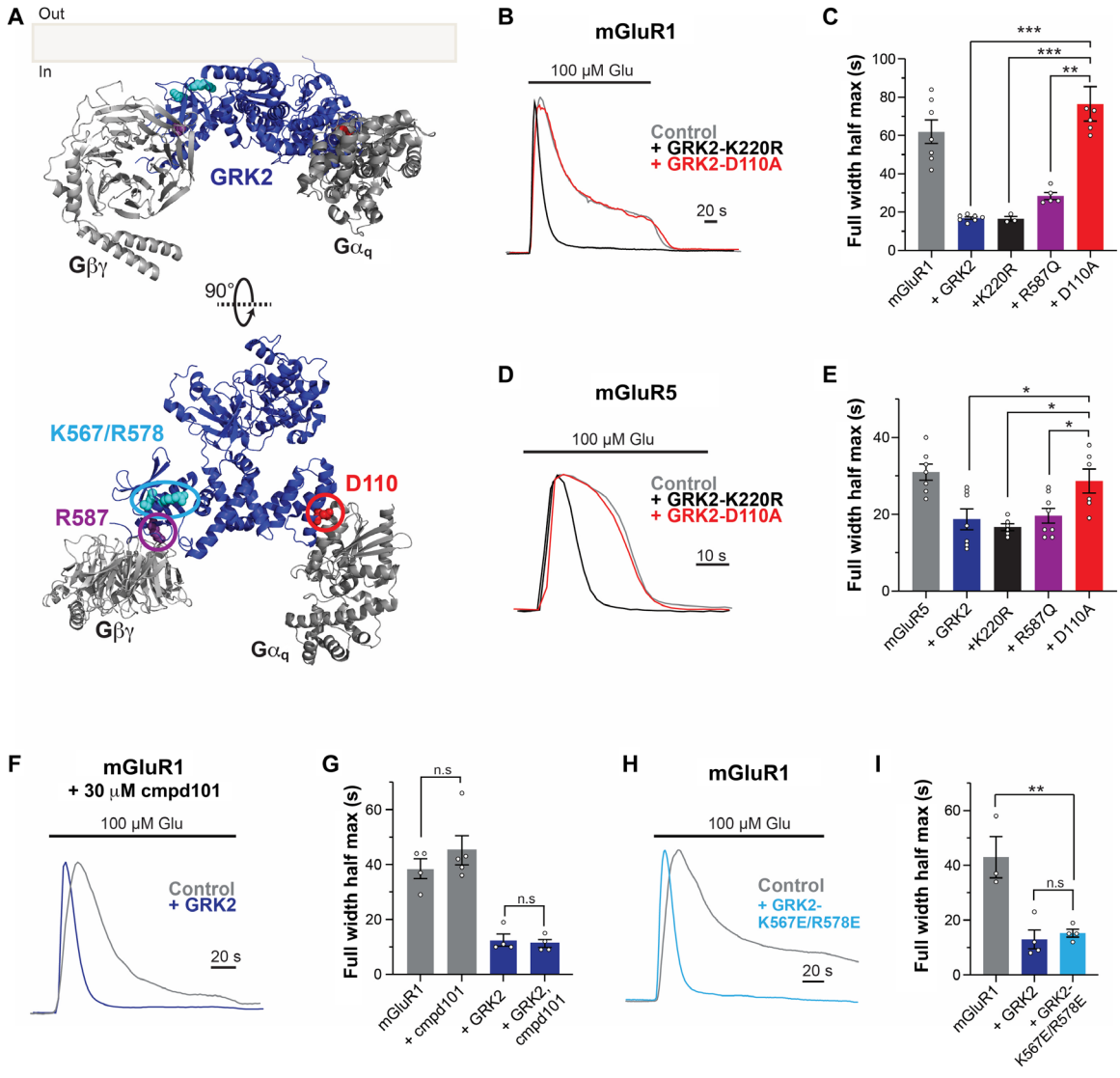


**Fig. 3. GRK2 effects on group I mGluR $Ca^{2+}$ responses are dependent on $G\alpha_q$ binding, but insensitive to GRK2/3 kinase inhibitors and impaired phospholipid binding.** (**A**) Structural snapshots showing architecture of GRK2, including residues involved in binding Gβγ (purple), phospholipids (cyan), and $G\alpha_q$ (red) (PDB: 1OMW). (**B** to **E**) Representative normalized average traces (B and D) and summary bar graphs (C and E) showing the effects of active site (K220R) and G protein–binding site (R587Q and D110A) GRK2 mutations on FWHM of responses to mGluR1 or mGluR5 activation. (**F** and **G**) Representative normalized, average traces (F) and summary bar graph (G) showing the lack of effect of saturating cmpd101 on the FWHM of glutamate responses in the absence or presence of overexpressed GRK2. (**H** and **I**) Representative normalized, average traces (H) and summary bar graph (I) showing the lack of effect of double mutation to the GRK2 phospholipid binding site on the ability of GRK2 to reduce the FWHM of glutamate responses. Each point represents an independent measurement; all graphs come from two to three separate experimental days, and error bars represent SEM. One-way ANOVA with Tukey's multiple comparisons tests. *$P < 0.05$, **$P < 0.01$, and ***$P < 0.001$.

states ($G_2$), would serve as a minimal model that reproduces the slowly desensitizing response to agonist under control conditions (see Materials and Methods for details). In the presence of GRK2, a fourth state ($G_3$) was added to compete with $G_1$, thereby providing a new route to deactivate the $Ca^{2+}$ signal on a faster time scale (Fig. 4, E and F). This kinetic model could reasonably capture the measured calcium signal time courses in the presence and absence of GRK2, including the acceleration of both the ON and OFF kinetics, with a minimal number of free parameters while forgoing a detailed description of the various chemical species and the nonlinear dynamics of $IP_3$-triggered calcium release from ER stores (*42*, *43*). A simple explanation for the shortening of the rise time arises from the fact that the ensemble time constants are functions of all the transition rates rather than pure measures of individual transition rates. In short, by accelerating the desensitization kinetics, GRK2/3 essentially blunt the rise and start the drop more quickly than it would in the absence of G protein scavenging.

To examine the potential competition between GRK2 and PLC for $G\alpha_q$-GTP, an equilibrium competition model was solved numerically across a range of possible values for affinity and abundance (Fig. 4, G and H). The fractions of $G\alpha_q$-GTP bound to GRK2 and PLC were plotted as a function of GRK2 concentration while systematically varying the PLC concentration for two distinct PLC-binding affinities (5 and 200 nM) based on previous binding studies (*28*, *65*–*67*)

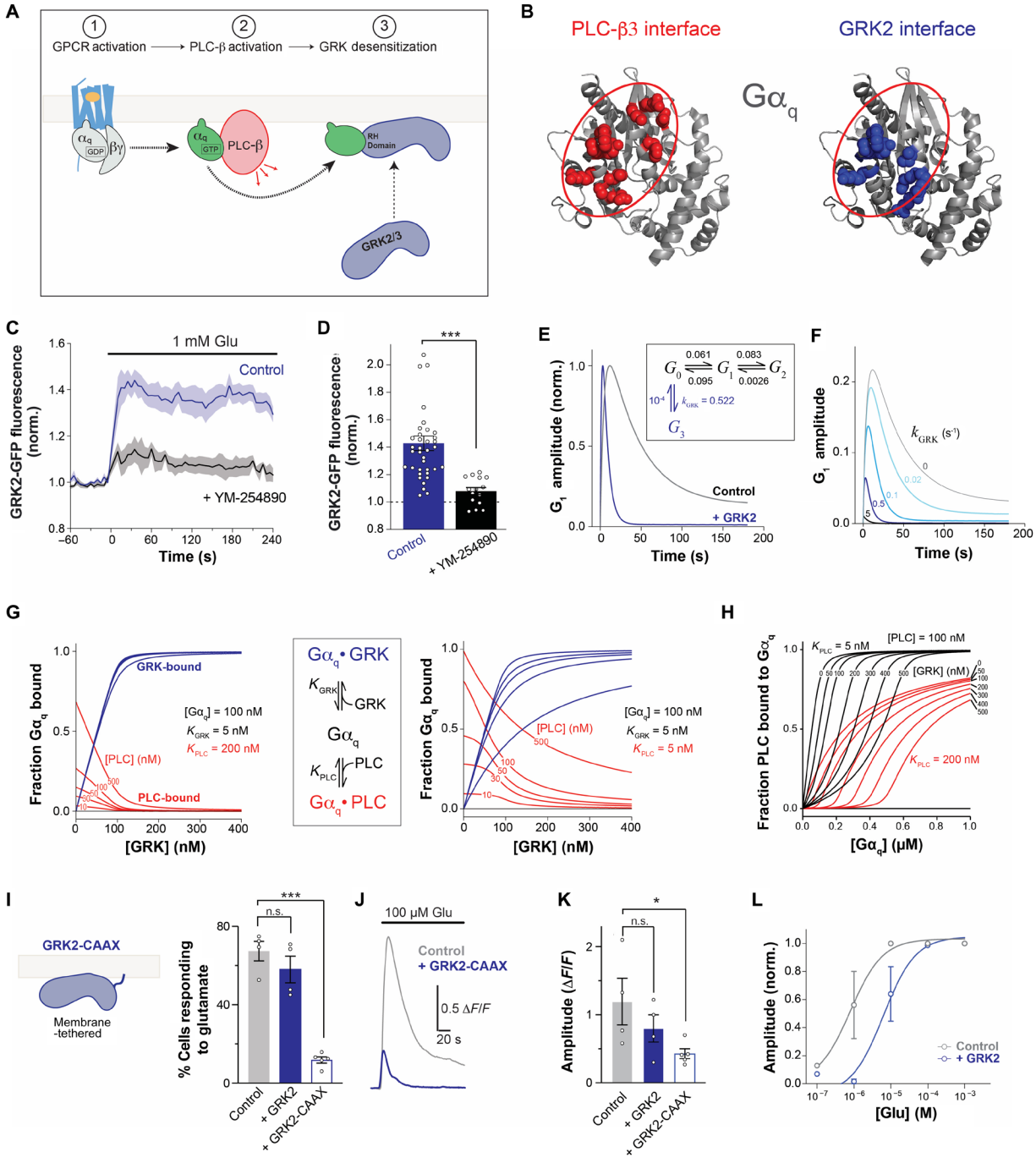


**Fig. 4. $G\alpha_q$/GRK2 binding underlies a working model of rapid desensitization.** (**A**) Schematic illustrating $G\alpha_q$-GTP sequestration by GRK2 to desensitize PLC-β activation. (**B**) Overlapping binding sites for PLC-β and GRK2 on $G\alpha_q$ (PDB: 2BCJ). (**C**) Fluorescence intensity of GRK2-GFP (normalized to baseline) during TIRF microscopy time lapse. YM-254890 (20 μM) was applied 30 min before imaging and present during acquisition. (**D**) Norm. GRK2-GFP fluorescence at $t = 3$ min after glutamate addition. Control, $n = 37$ cells; YM-254890, $n = 15$ cells. Two-tailed Student's $t$ test with Welch's correction. (**E**) Normalized $G\alpha_q$-triggered $Ca^{2+}$ transients fit to a simple four-state (blue) or a three-state (black) kinetic model in the presence or absence of GRK2. (**F**) A nonnormalized family of $Ca^{2+}$ responses generated using the four-state kinetic model while varying the $G_0 \rightarrow G_3$ rate constant ($k_{GRK}$) to mimic increasing GRK2 concentrations. (**G**) Equilibrium values of $G\alpha_q$ bound to GRK (blue) and PLC (red) computed for a variety of PLC and GRK concentrations for low-affinity (left) and high-affinity (right) PLC binding at a fixed concentration of $G\alpha_q$ and GRK affinity. (**H**) Using the equilibrium binding model, the fraction of PLC bound to $G\alpha_q$ plotted versus total $G\alpha_q$ concentration for a family of GRK concentrations with high-affinity (black) or low-affinity (red) PLC binding. (**I**) Schematic (left) and summary bar graph (right) showing the percentage of mGluR1-transfected cells responding to glutamate under control, GRK2, or GRK2-CAAX conditions. (**J** and **K**) Representative nonnormalized traces (J) and summary bar graph (K) showing the effects of GRK2-CAAX on R-GECO response amplitudes. (**L**) Dose-response curves for mGluR1-driven $Ca^{2+}$ responses to glutamate with or without GRK2 coexpression. Each point represents an independent measurement; all graphs come from two to four separate experimental days, and error bars represent SEM. For (D): unpaired $t$ test; for (H) and (K): two-way ANOVA with Tukey's multiple comparisons test. $^*P < 0.05$ and $^{***}P < 0.001$.

(Fig. 4G). We modeled the GRK2 affinity of $G\alpha_q$-GTP (5 nM) based on two prior studies (*28*, *68*). The fraction of $G\alpha_q$-GTP bound to PLC was plotted versus total $G\alpha_q$-GTP over the same range of GRK2 concentration to show that, at equilibrium, increasing local GRK2 abundance could strongly suppress $G\alpha_q$-GTP signaling via PLC over a remarkably wide range of concentrations and affinities. These kinetic and equilibrium schemes support a parsimonious competition model for the observed inhibitory effects of GRK2 expression on $G\alpha_q$ signaling.

Our kinetic and equilibrium competition modeling suggests some features of GRK2-mediated regulation of $G\alpha_q$ signaling. First, increasing levels of GRK2 should lead to a decrease in response amplitude to the point where $Ca^{2+}$ responses to glutamate are fully prevented with sufficient GRK2 levels. In our kinetic model, increasing the local abundance of GRK2 would increase the transition rate from $G_0$ to $G_3$ without affecting the other rate constants, resulting in accelerated deactivation kinetics and a smaller peak response (Fig. 4F). We tested this by tethering GRK2 to the membrane using a GRK2-CAAX construct that uses a C-terminal prenylation sequence (*69*) to increase the effective plasma membrane concentration of GRK2. While GRK2 coexpression had no clear effect on the percentage of cells responding to glutamate, GRK2-CAAX markedly reduced this from ~70 to ~20% (Fig. 4I). Among the cells that did respond, there remained a clear effect on FWHM and a substantial >50% decrease in amplitude (Fig. 4, J and K). These data indicate that GRK2 expression level and localization are key determinants of both the ability of cells to respond to GPCR activation at all and the amplitude and timing of the response. Furthermore, our modeling suggests that GRK2 decreases the amount of PLC-bound $G\alpha_q$ across $G\alpha_q$ concentrations (Fig. 4H), which should produce a right shift in the agonist dose-response curve. For this measurement, we turned to JRCaMP1b, a red, genetically encoded $Ca^{2+}$ sensor with a lower affinity for $Ca^{2+}$ than R-GECO (~300 versus ~700 nM) (*70*), which should limit underestimation of signal amplitude due to fluorescence saturation at micromolar $Ca^{2+}$ levels that may occur upon $G\alpha_q$-coupled GPCR activation (*42*, *43*). As predicted, coexpression of GRK2 shifted the glutamate dose response ~10-fold (Fig. 4L), indicating that GRK2 serves as a buffer to raise the threshold for a large signaling response.

On the basis of our model, we next predicted that other $G\alpha_q$-dependent signaling processes should be sensitive to GRK2 in a kinase-independent way. We tested this by measuring the activation of mitogen-activated protein kinase (MAPK) signaling by mGluR5 following glutamate application using a standard Western blot assay with antibodies to phosphorylated or total extracellular signal–regulated kinase 1/2 (ERK1/2). mGluR5 activation produced a clear response to glutamate that peaked at 5 min after glutamate application (Fig. 5, A and B). Coexpression of GRK2 substantially reduced this response such that the peak was decreased by >30% (Fig. 5, B and C). A similarly decreased response was observed with GRK2-K220R, showing that kinase-independent GRK2-mediated desensitization can have downstream consequences beyond the initial $Ca^{2+}$ response to $G\alpha_q$ activation (Fig. 5, B and C). In contrast, GRK2-D110A did not alter the peak ERK response to glutamate (Fig. 5, B and C), indicating both that $G\alpha_q$-GTP is an upstream driver of ERK phosphorylation and that $G\alpha_q$ binding is key for the inhibitory effect of GRK2.

Last, given that direct GRK2/GPCR interaction is not required for our model of signaling desensitization, we hypothesized that the rapid desensitization of $Ca^{2+}$ responses seen with group I mGluRs would be generalizable across $G\alpha_q$-coupled receptors. We tested this with both the 5-$HT_{2A}$R serotonin receptor and the $M_3$R muscarinic acetylcholine receptor, two prominent neuromodulatory GPCRs. Both receptors produced clear slowly desensitizing $Ca^{2+}$ responses following application of their native agonist. Coexpression of GRK2, but not GRK2-D110A, markedly reduced the FWHM for the responses of each receptor (Fig. 5, D to G). As seen with group I mGluRs, the ON kinetics of the 5-$HT_{2A}$R responses was accelerated (fig. S6, A and B), but such an effect was not observed with $M_3$Rs (fig. S6, C and D), which showed faster responses than the other GPCRs tested under control conditions. To assess the role of endogenous GRK2/3 levels on endogenous $G\alpha_q$-coupled GPCR signaling, we measured $Ca^{2+}$ responses to ATP application to stimulate $P_{2Y}$Rs that are natively expressed in HEK293 cells (*71*, *72*). As with heterologously expressed receptors (Figs. 1, I to L, and 5, D to G), the FWHM (Fig. 5, H and I) and rise time (fig. S6, E and F) of ATP responses were increased in GRK2/3 KO cells as compared with parental HEK293 cells. These data indicate that rapid, kinase-independent desensitization is a general feature of $G\alpha_q$-coupled receptor signaling, but kinetic differences can be seen across different GPCRs.

### Regulation of GPCR signaling cross-talk by GRK2

While noncanonical G protein–independent mechanisms exist (*73*, *74*), the vast majority of GPCRs signal through four families of heterotrimeric G proteins: $G\alpha_{i/o}$, $G\alpha_s$, $G\alpha_{q/11}$, and $G\alpha_{12/13}$. While some GPCRs can couple to multiple subfamilies (*75*), in most cases, there is a strong preference for one G protein family, and this is a key determinant of the biology of each receptor. However, multiple GPCR subtypes that couple to each G protein pathway can be present and coactivated within the same cell. One proposed mechanism of cross-talk between pathways depends on the binding of Gβγ subunits to PLC-β that does not directly activate the enzyme but can allosterically enhance the activation produced by $G\alpha_q$ binding (*10*, *76*). This mechanism may explain noncanonical $G\alpha_{i/o}$-coupled GPCR-driven $Ca^{2+}$ responses that have been observed in physiological systems, including muscle cells, cancer cells, osteoblasts, neurons, and platelets (*9*, *10*, *77*–*79*). After establishing that GRKs rapidly bind G proteins to shape $Ca^{2+}$ signaling dynamics (Figs. 1 to 5), we asked whether GRKs can also regulate the dynamics of this GPCR cross-talk.

We first coexpressed the $G\alpha_{i/o}$-coupled MOR with or without mGluR1 and observed robust DAMGO responses only in the presence of mGluR1 (Fig. 6A and fig. S7A). A similar mGluR1-dependent $Ca^{2+}$ response was observed upon activation of the $GABA_BR$, another $G\alpha_{i/o}$-coupled GPCR (fig. S7B). We reasoned that these responses are dependent on tonic $G\alpha_q$ activation by mGluR1 either via ligand-independent constitutive activity or low ambient levels of glutamate. Consistent with this, DAMGO-induced $Ca^{2+}$ responses were abolished in the presence of the mGluR1 NAM CPCCOEt (Fig. 6B and fig. S7C). To confirm that MOR responses were dependent on activation of $G\alpha_{i/o}$ and Gβγ release, we validated that they were blocked by the $G\alpha_{i/o}$-specific pertussis toxin (PTX) and the Gβγ inhibitor gallein (Fig. 6B). Together, these data argue that $G\alpha_{i/o}$-coupled GPCRs can drive $Ca^{2+}$ responses that are dependent on both $G\alpha_q$ and Gβγ.

On the basis of the above results, we hypothesized that the Gβγ and $G\alpha_q$ binding ability of GRK2 would inhibit this cross-talk and, as observed with direct $G\alpha_q$-receptor activation (Figs. 1 to 5), alter the timing of $Ca^{2+}$ responses. When GRK2 was coexpressed with MOR and mGluR1, the proportion of cells showing DAMGO $Ca^{2+}$

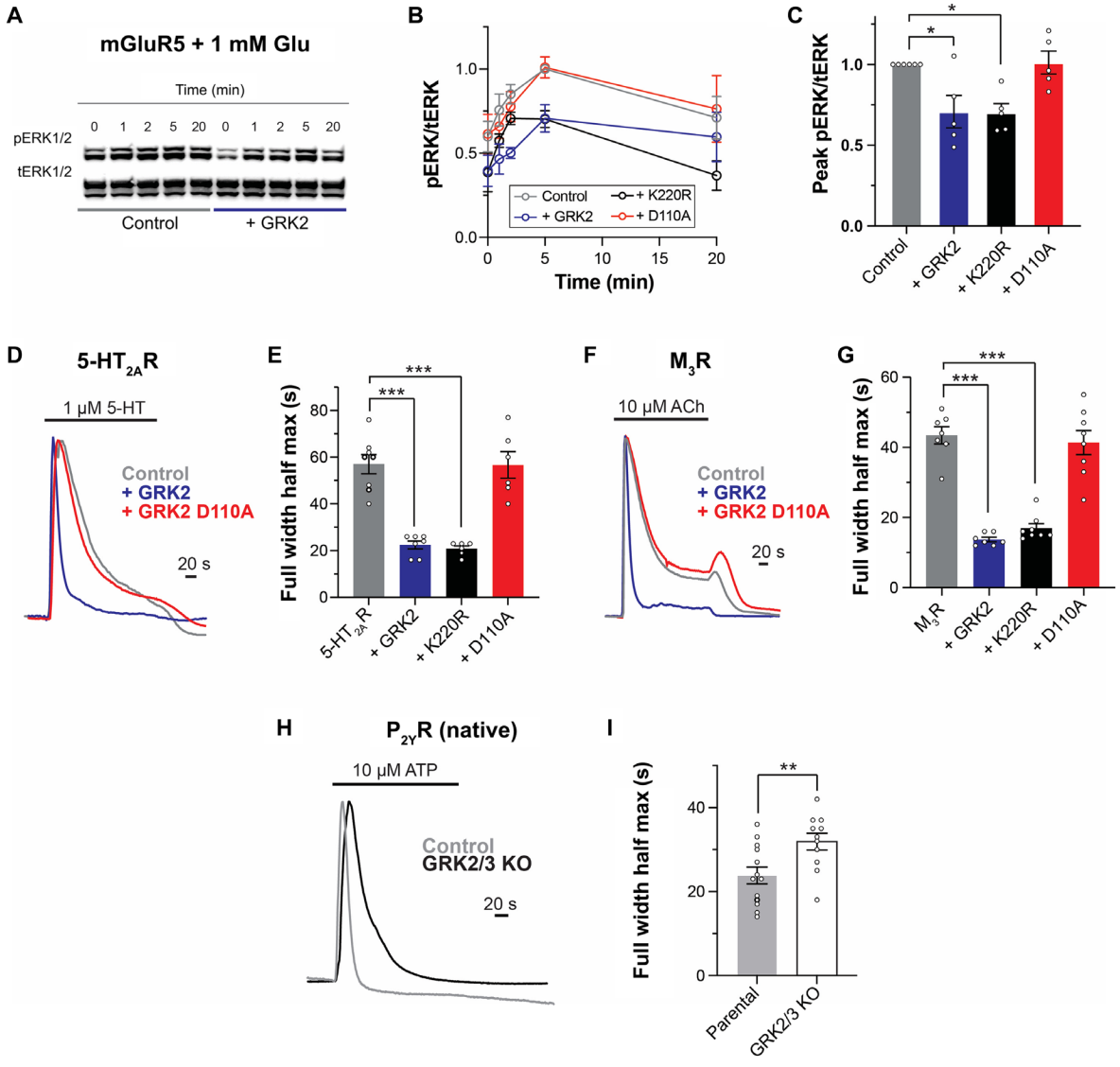


**Fig. 5. GRK2-mediated, $G\alpha_q$ binding-dependent desensitization of other effectors and other $G\alpha_q$-coupled receptors.** (**A** and **B**) Representative blot (A) and summary time course (B) showing the ERK phosphorylation response to glutamate in the absence or presence of GRK2. (**C**) Summary bar graph showing the peak, normalized pERK response to glutamate. (**D** and **E**) Representative normalized average traces (D) and summary bar graph (E) of FWHM showing the effects of GRK2 co-expression on R-GECO response to activation of the 5-$HT_{2A}$R. (**F** and **G**) Same as (D) and (E) but for the $M_3$R. (**H** and **I**) Representative normalized average traces (H) and summary bar graph (I) of FWHM showing the effects of GRK2/3 double KO on R-GECO response to activation of endogenous $P_{2Y}$Rs. Each point represents an independent measurement; all graphs come from two to five separate experimental days, and error bars represent SEM. For (I): unpaired *t* test; for (C), (E), and (G): one-way ANOVA with Tukey's multiple comparisons tests. *$P < 0.05$, **$P < 0.01$, and ***$P < 0.001$.

responses were markedly reduced, and the remaining responses showed accelerated desensitization with a threefold decrease in FWHM (Fig. 6, C to F). We tested GRK2 mutants that revealed that GRK2 inhibition of $G\alpha_{i/o}/G\alpha_q$ cross-talk is kinase independent and involves binding of both $G\beta\gamma$ and $G\alpha_q$, as only upon R587Q/D110A double mutation were DAMGO responses restored to control levels and durations (Fig. 6, C to F). To test whether endogenous levels of GRK2/3 can control this form of cross-talk, we again turned to GRK2/3 double KO cells. We found a clear increase in the percentage of cells responding to DAMGO in mGluR1 and MOR coexpressing cells in GRK2/3 KO compared to parental controls (fig. S7D). Furthermore, compared to parental cells, the relative DAMGO response amplitude was larger in GRK2/3 KO cells, supporting the idea that GRK2/3 serve as native regulators (fig. S7, E to G).

Last, we extended our analysis to the 5-$HT_{2A}$R, which also enabled DAMGO-driven $Ca^{2+}$ responses upon MOR coexpression. However, compared to mGluR1, a much lower percentage of cells showed clear responses (fig. S7H). We reasoned that the 5-$HT_{2A}$R may provide less $G\alpha_q$ tone than mGluR1 and, thus, tested whether low concentrations of 5-HT would enhance MOR responses. We found that application of 1 nM 5-HT failed to produce reliable responses on its own, but coapplication enabled robust DAMGO responses (Fig. 6, G and H, and fig. S7H). Coexpression of GRK2 or

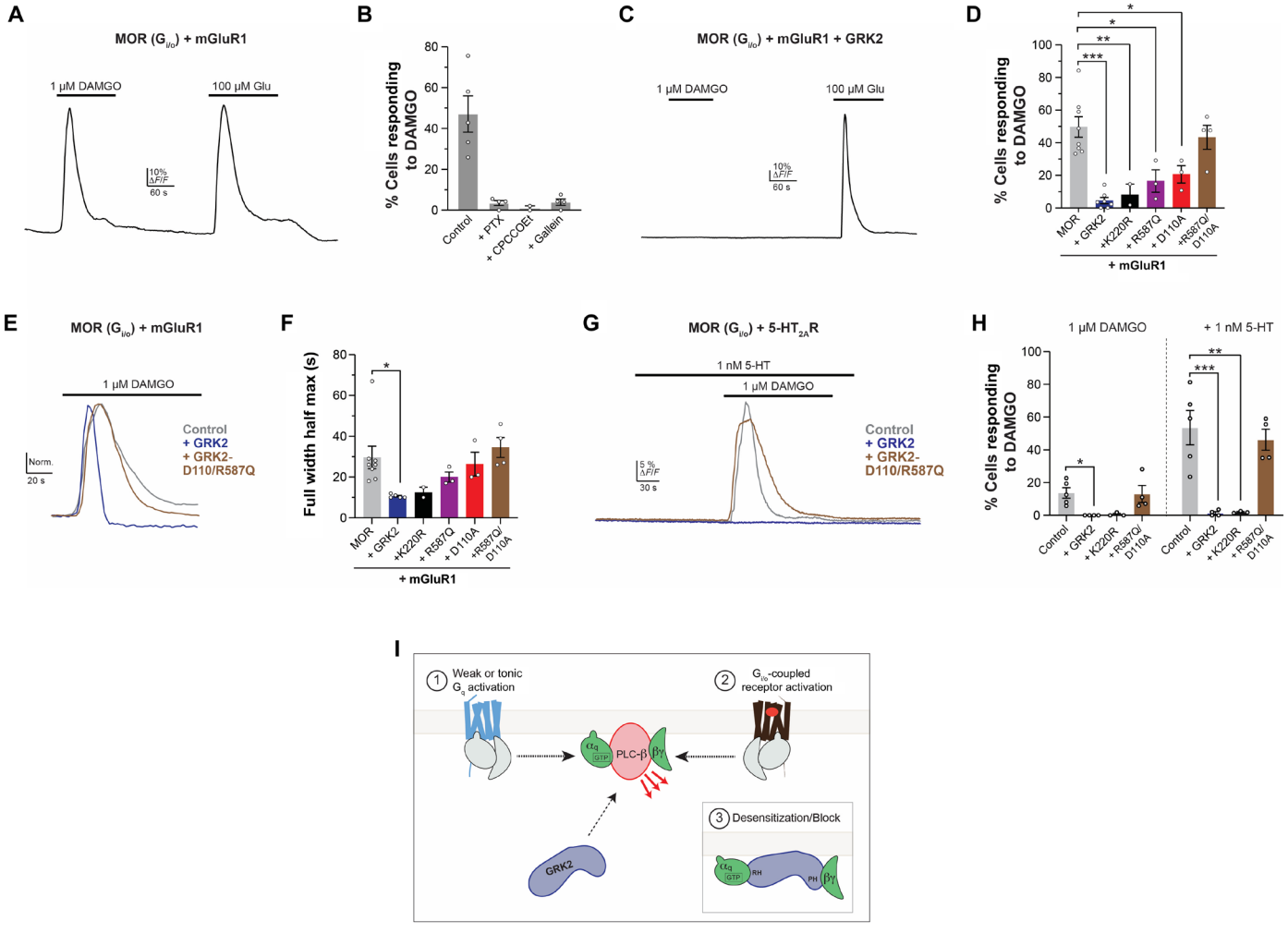


**Fig. 6. GRK2/G protein binding regulates cross-talk between $G_q$ and $G_{i/o}$-coupled GPCRs.** (**A**) Representative average trace showing that activation of the MOR ($G\alpha_{i/o}$-coupled) by the agonist DAMGO drives robust R-GECO responses when mGluR1 is coexpressed. (**B**) Summary bar graph showing the effects of PTX coexpression, mGluR1 NAM treatment (CPCCOEt, 100 μM), or Gβγ inhibitor (gallein, 10 μM, preincubated for 20 min). (**C** and **D**) Representative average trace (C) and summary bar graph (D) showing the effects of GRK2 coexpression on DAMGO responses. (**E** and **F**) Representative average traces (E) and summary bar graph (F) showing the effects of GRK2 on the FWHM of DAMGO responses. (**G** and **H**) Representative average trace and summary bar graph showing DAMGO-driven $Ca^{2+}$ responses in the presence of the $5\text{-}HT_{2A}R$ and 5-HT in the presence or absence of heterologously expressed WT or mutant GRK2. (**I**) Working model of GRK2-mediated inhibition of cross-talk–driven $Ca^{2+}$ responses to $G\alpha_{i/o}$ activation. Each point represents an independent measurement; all graphs come from two to three separate experimental days, and error bars represent SEM. One-way ANOVA with Tukey's multiple comparisons tests. $^*P < 0.05$, $^{**}P < 0.01$, and $^{***}P < 0.001$.

GRK2-K220R, but not GRK2-R587Q/D110A, was able to markedly decrease responses to both DAMGO alone and DAMGO in the presence of 5-HT (Fig. 6, G and H, and Fig. S7I), suggesting that GRK2 blunting of GPCR cross-talk is not receptor specific. Together, these data suggest that GRK2/3 may play a general G protein–buffering role to prevent or limit cross-talk between G protein families (Fig. 6I).

### GRK2-mediated, G protein–dependent GPCR internalization cross-talk

The ability of GPCRs to recruit GRK2 to the membrane via G proteins (*26*) (Fig. 4C) raises the possibility that $G\alpha_q$-mediated GRK recruitment contributes to receptor internalization and may enable cross-talk at the level of GRK-mediated internalization. We hypothesized that mGluR1, despite insensitivity to GRK2 in terms of its own internalization (Fig. 7A; see Materials and Methods), can enhance the GRK2-dependent internalization of other GPCRs. We first assayed internalization of the MOR ($G\alpha_{i/o}$-coupled) and $5\text{-}HT_{2A}R$ ($G\alpha_q$-coupled) and found that agonist-dependent internalization of either receptor is enhanced by GRK2 coexpression and reduced by coexpression of kinase-dead GRK2-K220R, which acts as a dominant negative (Fig. 7, B and C). The enhancement of $5\text{-}HT_{2A}R$ internalization, but not MOR internalization, by GRK2 was decreased when the D110A mutation was incorporated, indicating that $G\alpha_q$ binding contributes to GRK2-mediated receptor internalization (Fig. 7, B and C). Both $5\text{-}HT_{2A}R$ and MOR were sensitive to the R587Q mutation, consistent with a general role for Gβγ, albeit with a larger effect for the MOR (Fig. 7, B and C). Furthermore, treatment with YM-254890 impaired internalization of the $5\text{-}HT_{2A}R$, but not the MOR (fig. S8, A and B). In contrast, treatment with PTX impaired

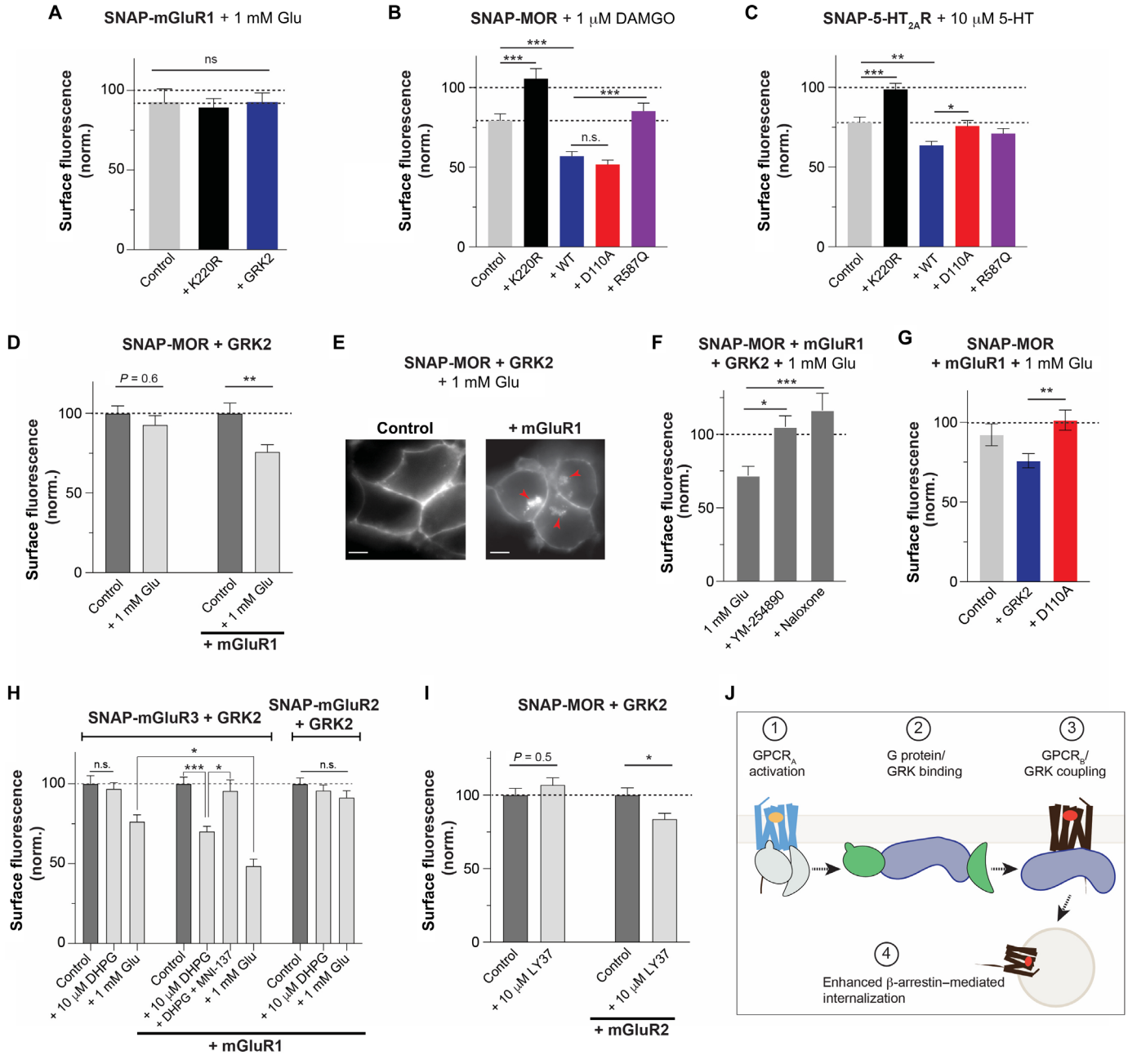


**Fig. 7. GRK2/G protein binding enables cross-internalization of coexpressed GPCRs.** (**A** to **C**) Surface labeling assay showing minimal agonist-induced internalization of mGluR1 (A) but clear GRK2-dependent internalization of the MOR (B) and 5-$HT_{2A}$R (C). 5-$HT_{2A}$R, but not MOR, is sensitive to the GRK2-D110A mutation that impairs $G\alpha_q$ binding. (**D** and **E**) Coexpression of mGluR1 enables glutamate-driven MOR internalization, as seen with surface labeling assay (D) and cell imaging (E). Scale bar, 10 μm. (**F**) Glutamate-driven MOR internalization is blocked by the $G\alpha_q$ inhibitor YM-254890 and the MOR antagonist naloxone. (**G**) GRK2-D110A is unable to mediate GRK2-dependent, glutamate-driven MOR internalization. (**H**) Effects of mGluR1 coexpression on internalization of mGluR3 or mGluR2. mGluR1 coexpression enables DHPG-driven mGluR3 internalization and enhances glutamate-driven mGluR3 internalization but does not enable mGluR2 internalization. (**I**) mGluR2 coexpression enables LY379268 (mGluR2/3 agonist)–driven internalization of MOR. (**J**) Working model of GRK2/$G\alpha_q$-driven GPCR cross-internalization. All graphs come from two to three separate experimental days, and error bars represent SEM. For (D) to (I): unpaired *t* test; for (A) to (C) and (F) to (H): two-way ANOVA with Tukey's multiple comparisons test. $^*P < 0.05$, $^{**}P < 0.01$, and $^{***}P < 0.001$.

internalization of the MOR, but not the 5-$HT_{2A}$R (fig. S8C, D). Coexpression of GRK mutants or PTX did not alter basal surface levels for the MOR or 5-$HT_{2A}$R (fig. S8, E and F). Together, these data indicate that $G\alpha_q$/GRK2 interaction can contribute to receptor internalization in a subtype-specific manner.

On the basis of the ability of G protein binding to contribute to GRK2-mediated internalization, we reasoned that agonist-driven GRK2 recruitment to the plasma membrane could enhance the internalization of other GPCRs. We tested this by coexpressing mGluR1 and GRK2 while measuring MOR surface levels. Activation

of mGluR1 by glutamate produced internalization of the MOR in the absence of an opioid agonist (Fig. 7D). This glutamate-dependent MOR internalization was dependent on mGluR1 expression (Fig. 7D) and could be visualized by labeling SNAP-MOR before glutamate treatment (Fig. 7E and fig. S9A). mGluR1-driven MOR internalization was blocked by either YM-254890 or the MOR antagonist naloxone (Fig. 7F), indicating that both $G\alpha_q$ activation and constitutive MOR activity are required. Glutamate-induced MOR internalization was dependent on GRK2 coexpression and reduced by incorporation of the D110A mutation (Fig. 7G), supporting a role for GRK2-$G\alpha_q$ interaction. Glutamate-driven mGluR1 internalization was not enhanced by MOR coexpression (fig. S9B), demonstrating that cointernalization of an mGluR1/MOR complex is not involved. mGluR1 coexpression also enhanced low-dose (10 nM) DAMGO-induced internalization of MOR (fig. S9C). This enhancement was blocked by either YM-254890 or the mGluR1 NAM CPCCOEt (fig. S9C), indicating that it was driven by constitutive mGluR1 activation, as was seen with $G\alpha_{i/o}$-driven $Ca^{2+}$ responses. mGluR1-driven internalization of MOR could also be initiated with DHPG and was abolished in β-arr1/2 double KO cells (fig. S9D), consistent with a central role for β-arrs in driving MOR endocytosis. We next asked whether endogenous levels of GRK2/3 were sufficient to mediate this form of cross-talk. In the absence of GRK2 overexpression, we found that glutamate produced a very modest decrease in surface MOR levels but was able to enhance the internalization induced by subsaturating 10 nM DAMGO (fig. S9E).

We asked whether this result could be generalized to other $G\alpha_{i/o}$-coupled receptors by testing the ability of mGluR1 to drive internalization of mGluR2 or mGluR3, two subtypes with which it does not efficiently heterodimerize (*8*, *80*). We previously showed that mGluR2 is resistant to agonist-driven internalization, while mGluR3 undergoes robust GRK2/3 and β-arr–driven internalization and endosomal trafficking (*25*). We first confirmed that the group I mGluR agonist, DHPG, did not drive internalization of mGluR3 when expressed alone (Fig. 7H). However, upon coexpression of mGluR1, DHPG drove robust mGluR3 internalization, which was blocked by the mGluR2/3 antagonist MNI-137 (Fig. 7H) or application of YM-254890 (fig. S9F). Furthermore, mGluR1 coexpression enabled a larger glutamate-driven internalization of mGluR3 (Fig. 7H). In contrast, mGluR2 remained resistant to internalization upon mGluR1 coexpression and treatment with DHPG or glutamate (Fig. 7H), confirming that an ability to couple to GRKs and β-arrs is required for this mode of cross-internalization. We previously showed that mGluR3 activation leads to membrane recruitment of β-arrs that is detectable by fluorescence imaging (*25*) (fig. S9G). We tested whether this would be observed upon mGluR1-mediated cross-regulation and found clear β-arr1–yellow fluorescent protein (YFP) membrane recruitment in response to DHPG only when mGluR3 and mGluR1 were coexpressed (fig. S9, G and H).

Last, we hypothesized that $G\alpha_{i/o}$-coupled GPCRs could also drive cross-internalization based on their ability to drive GRK2 recruitment via Gβγ (fig. S5A). We turned to mGluR2 because it does not undergo agonist-driven internalization itself (Fig. 7H) (*25*). However, as was observed with mGluR1 (Fig. 7D), mGluR2 agonism was able to drive a clear drop in MOR surface levels (Fig. 7I), which could be visualized with live-cell imaging (fig. S9, I and J). mGluR2-driven MOR internalization was blocked by PTX and dependent on an intact Gβγ binding site on GRK2 (fig. S9K). Together, these results show that the ability of a GPCR to drive G protein/GRK complex formation can enhance the internalization of other GPCRs even, as in the case of mGluR1 or mGluR2, when that receptor does not efficiently internalize itself (Fig. 7J).

## DISCUSSION

This study reveals that GRK2/3 are key modulators of GPCR signaling across time scales via multiple modes of regulation that are dependent on $G\alpha_q$ binding. We first find that rapid GRK/$G\alpha_q$ binding can control signaling dynamics on the seconds time scale independently of kinase activity and β-arr coupling (Figs. 1 to 5). GRK2 or GRK3 shapes the response of group I mGluRs to agonists by accelerating the onset, desensitization, and recovery-from-desensitization kinetics. While these may be generally thought of as inhibitory effects, the enhanced recovery and accelerated onset kinetics induced by GRK2 may also contribute to maintenance of signal fidelity rather than merely blunting the receptor response. GRK2/3 can also serve as a signaling barrier to decrease constitutive activity, prevent the response to low agonist doses, or limit sensitivity to brief focal activations. This may serve to enhance the signal-to-noise ratio of a cellular response to ligand, reinforcing the idea that GRK2-mediated inhibition may play a role both in desensitizing and in refining G protein signaling. Our data are in line with prior studies of group I mGluRs that have shown kinase-independent functional inhibition by GRK2/3 (*39*, *41*). In addition to building on this work with dynamic and mechanistic information, we show that GRK2-mediated rapid desensitization is a generalizable phenomenon that likely can regulate any $G\alpha_q$-coupled receptor, as shown with the 5-$HT_{2A}$R, $M_3$R, and $P_{2Y}$R, and any $G\alpha_q$-dependent effector, as shown with ERK activation. Elevated $G\alpha_q$ signaling is capable of driving stress granule formation (*81*), is associated with various aspects of cancer (*82*–*84*), and may contribute to cardiovascular disease (*85*), motivating future studies of GRK2/3-mediated regulation across physiological and disease contexts.

The acute signaling effects of GRK2 may be explained with a simple binding model based on competition for $G\alpha_q$ between GRK and PLC-β. This model captures the key features of the system but is an oversimplification as other factors likely further shape GRK-mediated inhibition. For a deeper quantitative understanding, precise biophysical measurements of rate constants and binding cooperativity for the relevant complexes (e.g., GRK2/$G\alpha_q$; PLC-β/$G\alpha_q$) are needed. Furthermore, guanosine triphosphatase (GTPase) activity, including the GTPase-activating protein activity of PLC-β (*86*) and GRK2/3 (*28*), and plasma membrane dynamics of each component are necessary to incorporate into a comprehensive model. The latter may tune this system by altering the apparent GRK2/3 plasma membrane concentration and localization to signaling microdomains, which are both likely shaped by cellular morphology. For example, the increased surface-to-volume ratio seen in neuronal or astrocytic processes may increase the extent of constitutive GRK2-mediated regulation of $G\alpha_q$ signaling. Together, our model argues that the relative expression levels of the GPCR, $G\alpha_q$, GRK2/3, and PLC-β subtypes are the major determinants of this regulation, providing a means of tuning $G\alpha_q$ signaling dynamics across cells. Consistent with this, GRK2/3 expression levels are highly variable across cells and dynamic within a given cell (*87*). Our data show that GRK2-driven desensitization of $G\alpha_q$-driven $Ca^{2+}$ responses is partially insensitive to disruption of the Gβγ and phospholipid-binding sites on GRK2 under our conditions. This is in contrast with prior work showing

that rapid GRK2-driven desensitization of GIRK currents is dependent on intact binding sites for both Gβγ and phospholipids. Furthermore, in contrast to the receptor specificity seen with GRK2-mediated GIRK current desensitization (*24*, *25*), the GRK2-mediated $Ca^{2+}$ desensitization observed here was not specific for GPCR subtypes. While both desensitization processes likely involve competition between effector and GRK2 for G proteins, this suggests differences in the underlying mechanisms and dynamic range of effects for each form of regulation. It is worth noting that differences in the extent of kinetic effects of GRK2 were observed across $G\alpha_q$-coupled GPCRs, with effects on rise time for mGluRs and the 5-$HT_{2A}$R, but not the $M_3$R, which is likely due to distinct properties of each GPCR in terms of G protein activation and subcellular organization. Along these lines, direct complex formation between GPCR and GRK2/3, as has been proposed for mGluR1 (*38*, *40*), may contribute to the unique kinetic features seen for each receptor. Last, we find that the kinase independence of GRK2-mediated regulation of $G\alpha_q$ signaling leads to insensitivity to standard GRK2/3 kinase inhibitors such as cmpd101, motivating the development of alternative pharmacological or genetic approaches to study GRK2/3-mediated processes in native systems. Two recent studies used overexpression of the isolated RH domain of GRK2 in mechanistic analyses of cardiac hypertrophy (*88*) and astrocyte $Ca^{2+}$ signaling (*89*), respectively. However, it is worth noting that this approach merely uses the RH domain as a $G\alpha_q$ sponge and does not directly address the physiological role of GRK2 itself.

Beyond merely regulating the acute response to ligand, we also find that rapid GRK/G protein binding can control the extent and timing of signaling cross-talk between GPCRs (Fig. 6). This complements the recent proposal that $G\alpha_{i/o}/G\alpha_q$ synergy is mediated by allosteric effects of Gβγ on $G\alpha_q$-driven PLC-β activation (*10*) and a recent study showing that Gβγ binding controls the duration of $G\alpha_q$-driven PLC-β activation (*90*). In line with this work, GRK2 binding to both $G\alpha_q$ and Gβγ contributes to regulation of cross-talk with mutation to both interfaces required to restore $Ca^{2+}$ responses. This effect is in line with the notion that GRK2 not only inhibits $G\alpha_q$ signaling but also increases signal specificity and temporal fidelity. Such cross-talk, and its regulation by GRK2, is likely relevant across systems where cells can respond to complex patterns of multiple hormones, neuromodulators, or neurotransmitters. For example, there are reports of intracellular $Ca^{2+}$ release in response to $G\alpha_{i/o}$-coupled (*91*, *92*) or $G\alpha_s$-coupled (*93*) GPCRs in astrocytes, but little data exist about the underlying mechanisms of these noncanonical responses and if they are regulated by G protein buffering systems, such as GRK2/3. Prior studies showing similar signaling cross-talk have often attributed effects to GPCR heteromerization (*94*, *95*); however, the $G\alpha_{i/o}$-driven $Ca^{2+}$ responses shown in our study do not require any direct interaction between GPCRs. Heteromerization may enhance the efficiency of cross-talk to overcome GRK-mediated regulation by maximizing spatial overlap of $G\alpha_q$-GTP and Gβγ to target the same population of PLC-β. Generally, GRK2/3 may serve as a buffer to restrict GPCR signaling cross-talk and limit the extent of spatial signaling spread. In future studies, spatiotemporally resolved dual GPCR activation and imaging will be required to dissect this mechanism across systems.

Last, we find that in addition to shaping rapid signaling dynamics, the ability of GRK2 to bind $G\alpha_q$ can contribute both to homologous internalization of $G\alpha_q$-coupled GPCRs and to cross-internalization of bystander or coactive GPCRs (Fig. 7). The finding that activation or tonic/constitutive signaling of one GPCR can decrease responsiveness to other signals reveals a novel form of lateral inhibition such that activation of one GPCR broadly down-regulates the cell's responsiveness to other signals. For example, constitutively active $G\alpha_q$ mutants, as seen commonly in uveal melanoma (*96*), may lead to elevated GRK2 recruitment and subsequent down-regulation of other GPCRs via GRK2. Notably, a recent study showed that common disease-associated $G\alpha_q$ mutations remain capable of efficient GRK2 binding (*97*). The ability of $G\alpha_q$-coupled GPCR activation to drive cross-internalization of other GPCRs may also be relevant in the clinical context of extended pharmacological treatment such that down-regulation of GPCRs coexpressed with the target receptor may occur.

The finding that $G\alpha_q$/GRK2 binding can contribute to GPCR internalization, as we show with both the 5-$HT_{2A}$R and cross-internalization of mGluR3 or MOR via mGluR1, complements prior studies showing that Gβγ/GRK2 binding can contribute to GRK2-dependent receptor endocytosis (*63*, *98*). Such G protein–dependent GRK recruitment may complicate the development of biased ligands with high efficacy for either G protein or β-arr coupling. Furthermore, we also find that Gβγ-mediated GRK recruitment after activation of a $G\alpha_{i/o}$-coupled GPCR can enable a similar form of cross-internalization, as we show with mGluR2 and MOR. Our internalization data raise the question of how G protein activation contributes to receptor endocytosis. A comprehensive analysis of GRK2 recruitment via the $M_3$R showed that both Gβγ and $G\alpha_q$ contribute to GRK2 recruitment with a larger role for Gβγ but higher sensitivity to low agonist doses for $G\alpha_q$ (*26*). In line with this, we show using TIRF imaging that, compared to fully blocking G protein activation or impairing Gβγ binding, impairing the $G\alpha_q$ binding site only has a modest effect on GRK2 recruitment in the background of the Gβγ binding mutation. It is important to note that the dynamic range of the fluorescence changes observed in our TIRF measurements may obscure some of the effects of mutations and do not allow us to easily assess basal GRK2 recruitment, which may be dependent on $G\alpha_q$ binding. However, our data and those of others together suggest that $G\alpha_q$/GRK2 binding may play a role downstream of direct membrane recruitment to enhance the spatial targeting of GRK2 within critical membrane microdomains. This is consistent with single-molecule imaging studies showing that GPCR transducer coupling can occur in membrane hotspots (*99*) and the aforementioned $M_3$R study showing that GRK2/$G\alpha_q$ binding enhanced β-arr recruitment (*26*). A recent study of the angiotensin type II receptor found that $G\alpha_q$ activation can contribute to GRK2/3-driven β-arr recruitment and impair GRK5/6 coupling by controlling localization of these GRK subtypes to mobile versus immobile membrane phases (*50*). Last, $G\alpha_q$-dependent trafficking may also involve some of the wide variety of proteins that have been shown to bind GRK2, including caveolin and cytoskeletal proteins (*100*, *101*). Ultimately, this finding motivates future work to further delineate the underlying mechanisms and physiological effects of G protein–dependent trafficking cross-talk.

## MATERIALS AND METHODS

### Cell culture, molecular cloning, and gene expression

HEK293T cells were purchased from the American Type Culture Collection (ATCC; CRL-11268; CRL-1573), authenticated by Bio-Synthesis Inc. and tested negative for mycoplasma using the Universal Mycoplasma Detection Kit from ATCC. GRK2/3 double KO, β-arr1/2

double KO, and parental HEK293 cells were previously reported (*50*) and tested negative for mycoplasma using the Universal Mycoplasma Detection Kit from ATCC. Cells were maintained in Dulbecco's modified Eagle's medium (GIBCO) supplemented with 5% fetal bovine serum (FBS) and passaged by trypsin/EDTA digestion upon reaching ~95% confluency. Cells were maintained in a humidified incubator with 5% $CO_2$ at 37°C. HEK293T cells were plated on poly-L-lysine–coated coverslips (18 mm) or glass bottom dishes (35 mm for TIRF imaging) and transfected using Lipofectamine 2000 (Thermo Fisher) with a typical efficiency of ~70 to 80% of cells based on fluorescence. The following cDNA for bovine GRKs were used: untagged GRK2 (Addgene #14691), GRK3 (Addgene #32689), GRK5 (Addgene #14690), GRK6 (Addgene #32693), GRK2-GFP (*24*), and GRK2-CAAX (Addgene #166224). The following $Ca^{2+}$ indicator plasmids were used: R-GECO (*47*), JRCaMP1b (*70*), and ER-GCaMP (*51*). The following GPCR cDNA were used: SNAP-tagged mGluRs (*80*) (human mGluR1, mGluR5; rat mGluR2, mGluR3), rat SNAP-$5HT_{2a}$ (*102*), rat $GABA_{B1}$ and $GABA_{B2}$ (*22*), and rat SNAP-MOR (this study; N-terminal HA followed by SNAP-tag followed by full-length MOR). For most experiments, cells were maintained in antagonist after transfection to maintain cell health [1 μM 2-Methyl-6-(phenylethynyl)pyridine (MPEP) for mGluR5, 10 μM LY341495 for mGluR1 or mGluR3, 10 μM naloxone for MOR, and 10 μM ketanserin for 5-$HT_{2A}$R]. All experiments were performed 24 to 48 hours after transfection. For $Ca^{2+}$ imaging and ERK phosphorylation experiments, each coverslip received 0.5 μg of each receptor, 0.5 μg of the wild-type or mutant GRK [unless otherwise indicated, see Fig. 1 (I to L) and fig. S3], and, for some experiments, 0.4 μg of PTX-S1 (*103*). For $Ca^{2+}$ imaging, 0.2 μg of the relevant $Ca^{2+}$ indicator (R-GECO, ER-GCaMP6, or JR-CAMP1B) was cotransfected. For TIRF imaging experiments, each imaging dish received 1 μg of receptor, 0.5 μg of wild-type or mutant GRK2-GFP, and 1 μg of excitatory amino acid transporter 3 EAAT3 (gift of J. Mathiesen) to remove extracellular glutamate. For surface labeling or internalization experiments, cells were transfected with 0.5 μg of SNAP-tagged receptor (with 0.5 μg of untagged receptors for cross-talk studies) with or without 0.5 μg wild-type or mutant GRK2. For β-arr recruitment experiments, cells were cotransfected with 0.2 μg of β-arr1–YFP plasmids 48 hours before imaging. All point mutants were made using standard PCR-based site-directed mutagenesis.

## $Ca^{2+}$ imaging

HEK293T cells were imaged on an inverted microscope (Olympus IX83) with a 20× objective at room temperature in extracellular (EX) solution composed of the following: 135 mM NaCl, 5.4 mM KCl, 10 mM Hepes, 5 mM L-glucose, 2 mM $CaCl_2$, and 1 mM $MgCl_2$ (pH 7.4). R-GECO was excited using a 561-nm laser at 0.5 Hz, for most experiments, or 5 Hz for fast perfusion analysis (fig. S1, E to G), with a 100-ms exposure time. For experiments with gallein (Tocris, catalog no. 3090) or cmpd101 (Tocris, catalog no. 5642), cells were preincubated with 10 μM gallein or 30 μM cmpd101 for 20 min before imaging. ER-GCaMP6f was excited using a 488-nm laser at 0.5 Hz with a 100-ms exposure time. Time lapse movies were recorded with a scientific complementary metal–oxide–semiconductor (scMOS) camera (Hamamatsu ORCA-Flash4v3.0). For most experiments, a continuous gravity-driven perfusion system was used at a speed of 5 ml/min. For fast perfusion experiments (fig. S1, E to G), a pressurized perfusion system (Automate Scientific) was used at a speed of 20 to 30 ml/min as previously described (*104*). All agonists, antagonists, and PAMs were purchased from Tocris: DHPG (catalog no. 0805), LY341495 (catalog no. 1209), LY379268 (catalog no. 2453), VU0360172 (catalog no. 4323), Ro 67-7476 (catalog no. 4346), MPEP (catalog no. 1212), CPCCOET (catalog no. 1028), DAMGO (catalog no. 1171), Baclofen (catalog no. 0417), 5-HT (catalog no. 3547), and acetylcholine (catalog no. 2809). YM-254890 was purchased from Cayman Chemical Company (catalog no. 29735). For PORTL experiments, labeling of SNAP-mGluR2-mGluR5 was done with 10 μM $BGAG_{12,400}$ at 37°C for 45 to 60 min before imaging as previously described (*52*). Photoactivation experiments were performed at 30°C with continuous perfusion on a Zeiss LSM880 scanning confocal microscope using ZEN Black software with a 63× objective, a 488-nm laser for imaging, and a 405-nm laser for photoactivation. PORTL photoactivation was performed by scanning a 405-nm laser at 100% power in a defined region for 40 iterations between each imaging frame as described previously (*52*).

Image analysis was performed using ImageJ (Fiji) with manual identification of single-cell regions of interest and classification of cells as oscillatory (>1 peak during drug application) or nonoscillatory. Intensities were normalized to the baseline before drug application. FWHM was calculated for each independent movie as the width (duration of time, measured in seconds) of an average trace (40 to 80 cells) representing the $Ca^{2+}$ transient after drug application measured at half of its maximum amplitude. Peak amplitude was determined as the highest value of arbitrary unit fluorescence reached after drug application. Rise time was measured in seconds as the time from baseline to peak amplitude, and the $\tau_{desensitization}$ was determined using single exponential fits in GraphPad Prism. All conditions were repeated on at least two separate experimental days; see figure legends for details.

## Receptor imaging and internalization analysis

Surface labeling assay, internalization imaging, and β-arr recruitment were measured as previously described (*25*). For the surface labeling assay, cells were first incubated in EX with or without drugs for 30 min at 37°C and then labeled with 1 μM cell-impermeable BG-Alexa-546 (New England Biolabs) for 20 min at room temperature. Cells were imaged on an inverted microscope (Olympus IX83) with a 60× 1.49 numerical aperture (NA) objective using a 560-nm laser. Snapshots were taken to measure mean fluorescence intensity across multiple fields of view via ImageJ. For all transfection conditions, an agonist and no agonist (normalized to the 100 value) condition was included to enable direct comparisons of surface levels. For internalization assay, cells were first labeled with 1 μM BG-Alexa-546 for 20 min (New England Biolabs), then incubated in EX with or without drugs for 30 min, and imaged right after. The percentage of cells showing intracellular fluorescence was analyzed manually and blindly across multiple fields of view. For β-arr recruitment experiments, cells were treated with agonists for 15 min and then imaged with a 60× 1.49 NA objective using a 488-nm laser to excite YFP. The percentage of cells showing membrane recruitment was analyzed manually and blindly across multiple fields of view. For experiments with $G\alpha_q$ blocker, 20 μM YM-254890 was added to cells for 30 min before agonist treatment. Across all assays, conditions were repeated on at least two separate experimental days (see figure legends for details).

## TIRF imaging

To monitor agonist-driven plasma membrane recruitment of GRK2, we used a TIRF microscopy–based assay described previously (*27*).

Cells were washed and live imaged in Hepes-buffered saline imaging solution with 135 mM NaCl, 5 mM KCl, 0.4 mM $MgCl_2$,1.8 mM $CaCl_2$, 20 mM Hepes, and 5 mM D-glucose adjusted to pH 7.4. Time lapse image series were acquired at 37°C with 488-nm laser excitation using a 100× 1.49 oil CFI Apochromat TIRF objective on a Nikon TIRF microscope operated with NIS Element AR 5.21.03 and equipped with a temperature-controlled chamber (Okolab), perfect focus system, and an Orca Fusion BT sCMOS camera at 5-s intervals. Drugs were added by bath application at concentrations indicated in the figure legends. Protein relocalization was calculated as $R(t)/R_0$ with $R(t)$ being the fluorescence signal at each time point ($t$) and $R_0$ being the mean fluorescence signal of the 10 time points before agonist addition.

## Modeling

A minimal kinetic model was developed to aid understanding of GRK2 as a negative regulator of signaling via competition for $G\alpha_q$ without attempting to capture the detailed chemistry of several diffusing species and complex nonlinear dynamics of ER $Ca^{2+}$ release. We therefore developed a state model that reproduced the activation and inactivation kinetics of signaling as defined by intracellular $Ca^{2+}$ measurements in the presence and absence of GRK2 overexpression. Three signaling states were defined as $G_0$ (basal), $G_1$ (PLC active), and $G_2$ (inactive). Qualitatively, these states could correspond to active free $G\alpha_q$, $G\alpha_q$ bound to PLC, and an inactive $IP_3$/ER $Ca^{2+}$ reservoir, respectively. The measured $Ca^{2+}$ signal corresponds to $G_1$ in this scenario. In the presence of GRK2, a fourth state, $G_3$, was attached to $G_0$ representing the binding of GRK2 to free $G\alpha_q$ (Fig. 4E)

$$\left[G_3 \underset{k_4}{\overset{k_5}{\rightleftharpoons}}\right] G_0 \underset{k_1}{\overset{k_0}{\rightleftharpoons}} G_1 \underset{k_3}{\overset{k_2}{\rightleftharpoons}} G_2$$

$$\frac{dG_0}{dt} = -(k_0 + k_4)G_0 + k_1 G_1 + k_5 G_3$$

$$\frac{dG_1}{dt} = -(k_1 + k_2)G_1 + k_0 G_0 + k_3 G_2$$

$$\frac{dG_2}{dt} = -k_3 G_2 + k_2 G_1$$

$$\frac{dG_3}{dt} = -k_5 G_3 + k_4 G_0$$

These three- and four-state kinetic models were implemented using custom-written algorithms in Igor Pro 8 (Wavemetrics) using the Bulirsch-Stoer method with Richardson extrapolation for numerical integration. Fits to individual fluorescence traces were made by a global parameter search minimizing the mean squared error between the peak-normalized data and simulations. No attempt was made to model amplitude effects since we did not measure absolute intracellular $Ca^{2+}$ levels. $Ca^{2+}$ imaging data in the absence of GRK2 overexpression were first fit to a three-state model ($G_0$, $G_1$, and $G_2$) to determine the activation and inactivation rate constants ($k_4$ = $k_5$ = 0, in this case). The GRK-dependent state $G_3$ was then added to this model and fit using data collected from cells overexpressing GRK2. Because the steady-state fluorescence amplitude was small in the presence of GRK2, the modeling was relatively insensitive to the rate constant corresponding to recovery from the fourth state (rate constant $k_5$). This value was fixed to $10^{-4}$ per second for global parameter searches.

To describe an equilibrium-binding competition between PLC and GRK2 for $G\alpha_q$ using the simple scheme shown in Fig. 4F, two simultaneous coupled nonlinear equations were solved numerically

$$x^2 + xy - (K_G + A_T + G_T)x - G_T y + A_T G_T = 0$$

$$y^2 + xy - (K_P + A_T + P_T)x - P_T y + A_T P_T = 0$$

Then, the bound fractions $x/A_T$ and $y/A_T$ were plotted versus GRK2 for a variety of PLC concentrations and for two distinct PLC binding affinities assuming a GRK binding affinity of 5 nM and 100 nM total $G\alpha_q$ (Fig. 4F). Equilibrium values for $x$ and $y$ over a range of parameters were computed in Igor Pro using the built-in Jenkins-Traub algorithm. To assess the relative amount of PLC activity with a total PLC concentration of 100 nM, $y/P_T$ was plotted versus $A_T$ for a range of GRK2 concentrations and for two PLC binding affinities (5 versus 200 nM) (Fig. 4K).

| | |
|---|---|
| $A_T$ | total concentration of active $G\alpha_q$ |
| $G_T$ | total concentration of GRK2 |
| $P_T$ | total concentration of PLC |
| $K_G$ | dissociation constant for $G\alpha_q$ bound to GRK2 |
| $K_P$ | dissociation constant for $G\alpha_q$ bound to PLC |
| $x$ | concentration of $G\alpha_q$ bound to GRK2 |
| $y$ | concentration of $G\alpha_q$ bound to PLC |

## ERK phosphorylation

Heterologously expressed receptors from HEK293T cells were treated with 1 mM glutamate (or 1 μM MPEP for baseline time point), and lysis was performed at 4°C with Pierce radioimmunoprecipitation assay lysis buffer (89901) supplemented with Pierce protease and phosphatase inhibitors (A32955 and A32957). Protein extracts were quantified using a Pierce BCA protein assay kit (23225). Lysate samples containing 15 mg of protein were incubated for 5 min at 95°C with NuPAGE lithium dodecyl sulfate Sample Buffer and 0.25 M DL-dithiothreitol. Samples were loaded on a NuPAGE 4 to 20% tris-glycine gel (Thermo Fisher), and the chamber was filled with 1× NuPAGE Tris-Glycine SDS running buffer (Thermo Fisher) and run at 80 V for 2 hours. Samples were transferred in 1× NuPAGE transfer buffer (Thermo Fisher) at 350 mA for 2 hours at 4°C onto a Bio-Rad Immun-Blot polyvinylidene difluoride membrane (1620177). The membrane was rinsed in TBST buffer (20 mM tris, 150 mM NaCl, and 0.1% Tween 20) and then blocked for 1 hour in TBST containing 5% bovine serum albumin (BSA; GeminiBio, 700-100P) and 5% FBS (Gibco, 10437-028) at room temperature. The membrane was incubated at 4°C overnight in phospho-p44/42 MAPK (ERK1/2) antibody (Cell Signaling, 9101L) diluted 1:1000 in 3% BSA. The membrane was washed three times with TBST and then incubated in horseradish peroxidase–conjugated goat anti-mouse immunoglobulin G secondary antibody (Invitrogen, 31462) diluted 1:5000 in 3% BSA for 1 hour at room temperature. Membranes were then washed four times with TBST, incubated with Western-Bright ECL spray (Advansta, K-12049-D50), and then imaged using a Syngene G-Box Chemi XX6 imager. Membranes were stripped with mild stripping buffer [Abcam; 200 mM glycine, 3.5 mM SDS, and 1% Tween 20 (pH 2.2)], blocked (5% BSA + 5% FBS) for 1 hour at room temperature, and incubated in p44/42 MAPK (ERK1/2) antibody (Cell Signaling, 9102L) diluted 1:1000 in 3% BSA overnight at 4°C. Membranes were developed and imaged as described

above. Images were analyzed using ImageJ. Each condition was tested in at least five separate experiments.

## SUPPLEMENTARY MATERIALS

Supplementary material for this article is available at https://science.org/doi/10.1126/sciadv.abq3363

View/request a protocol for this paper from *Bio-protocol*.

## REFERENCES AND NOTES


1. M. Grundmann, E. Kostenis, Temporal bias: Time-encoded dynamic GPCR signaling. *Trends Pharmacol. Sci.* **38**, 1110–1124 (2017).
2. T. Patriarchi, J. R. Cho, K. Merten, M. W. Howe, A. Marley, W.-H. Xiong, R. W. Folk, G. J. Broussard, R. Liang, M. J. Jang, H. Zhong, D. Dombeck, M. von Zastrow, A. Nimmerjahn, V. Gradinaru, J. T. Williams, L. Tian, Ultrafast neuronal imaging of dopamine dynamics with designed genetically encoded sensors. *Science* **360**, eaat4422 (2018).
3. M. Jing, Y. Li, J. Zeng, P. Huang, M. Skirzewski, O. Kljakic, W. Peng, T. Qian, K. Tan, J. Zou, S. Trinh, R. Wu, S. Zhang, S. Pan, S. A. Hires, M. Xu, H. Li, L. M. Saksida, V. F. Prado, T. J. Bussey, M. A. M. Prado, L. Chen, H. Cheng, Y. Li, An optimized acetylcholine sensor for monitoring in vivo cholinergic activity. *Nat. Methods* **17**, 1139–1146 (2020).
4. J. Wan, W. Peng, X. Li, T. Qian, K. Song, J. Zeng, F. Deng, S. Hao, J. Feng, P. Zhang, Y. Zhang, J. Zou, S. Pan, M. Shin, B. J. Venton, J. J. Zhu, M. Jing, M. Xu, Y. Li, A genetically encoded sensor for measuring serotonin dynamics. *Nat. Neurosci.* **24**, 746–752 (2021).
5. J. T. Williams, S. L. Ingram, G. Henderson, C. Chavkin, M. von Zastrow, S. Schulz, T. Koch, C. J. Evans, M. J. Christie, Regulation of mu-opioid receptors: Desensitization, phosphorylation, internalization, and tolerance. *Pharmacol. Rev.* **65**, 223–254 (2013).
6. A. Paul, M. Crow, R. Raudales, M. He, J. Gillis, Z. J. Huang, Transcriptional architecture of synaptic communication delineates GABAergic neuron identity. *Cell* **171**, 522–539.e20 (2017).
7. P. A. Insel, K. Sriram, M. W. Gorr, S. Z. Wiley, A. Michkov, C. Salmerón, A. M. Chinn, GPCRomics: An approach to discover GPCR drug targets. *Trends Pharmacol. Sci.* **40**, 378–387 (2019).
8. J. Lee, H. Munguba, V. A. Gutzeit, D. R. Singh, M. Kristt, J. S. Dittman, J. Levitz, Defining the homo- and heterodimerization propensities of metabotropic glutamate receptors. *Cell Rep.* **31**, 107605 (2020).
9. M.-L. Rives, C. Vol, Y. Fukazawa, N. Tinel, E. Trinquet, M. A. Ayoub, R. Shigemoto, J.-P. Pin, L. Prézeau, Crosstalk between GABAB and mGlu1a receptors reveals new insight into GPCR signal integration. *EMBO J.* **28**, 2195–2208 (2009).
10. E. M. Pfeil, J. Brands, N. Merten, T. Vögtle, M. Vescovo, U. Rick, I.-M. Albrecht, N. Heycke, K. Kawakami, Y. Ono, F. M. N. Kadji, S. Hiratsuka, J. Aoki, F. Häberlein, M. Matthey, J. Garg, S. Hennen, M.-L. Jobin, K. Seier, D. Calebiro, A. Pfeifer, A. Heinemann, D. Wenzel, G. M. König, B. Nieswandt, B. K. Fleischmann, A. Inoue, K. Simon, E. Kostenis, Heterotrimeric G protein subunit Gαq is a master switch for gβγ-mediated calcium mobilization by Gi-coupled GPCRs. *Mol. Cell* **80**, 940–954.e6 (2020).
11. R. R. Gainetdinov, R. T. Premont, L. M. Bohn, R. J. Lefkowitz, M. G. Caron, Desensitization of G protein-coupled receptors and neuronal functions. *Annu. Rev. Neurosci.* **27**, 107–144 (2004).
12. S. Rajagopal, S. K. Shenoy, GPCR desensitization: Acute and prolonged phases. *Cell. Signal.* **41**, 9–16 (2018).
13. S. K. Shenoy, R. J. Lefkowitz, β-Arrestin-mediated receptor trafficking and signal transduction. *Trends Pharmacol. Sci.* **32**, 521–533 (2011).
14. M. von Zastrow, A. Sorkin, Mechanisms for regulating and organizing receptor signaling by endocytosis. *Annu. Rev. Biochem.* **90**, 709–737 (2021).
15. J. W. Wisler, S. M. De Wire, E. J. Whalen, J. D. Violin, M. T. Drake, S. Ahn, S. K. Shenoy, R. J. Lefkowitz, A unique mechanism of β-blocker action: Carvedilol stimulates β-arrestin signaling. *Proc. Natl. Acad. Sci. U.S.A.* **104**, 16657–16662 (2007).
16. L. M. Slosky, Y. Bai, K. Toth, C. Ray, L. K. Rochelle, A. Badea, R. Chandrasekhar, V. M. Pogorelov, D. M. Abraham, N. Atluri, S. Peddibhotla, M. P. Hedrick, P. Hershberger, P. Maloney, H. Yuan, Z. Li, W. C. Wetsel, A. B. Pinkerton, L. S. Barak, M. G. Caron, β-Arrestin-biased allosteric modulator of NTSR1 selectively attenuates addictive behaviors. *Cell* **181**, 1364–1379.e14 (2020).
17. A. Manglik, H. Lin, D. K. Aryal, J. D. McCorvy, D. Dengler, G. Corder, A. Levit, R. C. Kling, V. Bernat, H. Hübner, X.-P. Huang, M. F. Sassano, P. M. Giguère, S. Löber, D. Duan, G. Scherrer, B. K. Kobilka, P. Gmeiner, B. L. Roth, B. K. Shoichet, Structure-based discovery of opioid analgesics with reduced side effects. *Nature* **537**, 185–190 (2016).
18. Z. Shao, Q. Shen, B. Yao, C. Mao, L.-N. Chen, H. Zhang, D.-D. Shen, C. Zhang, W. Li, X. Du, F. Li, H. Ma, Z.-H. Chen, H. E. Xu, S. Ying, Y. Zhang, Identification and mechanism of G protein-biased ligands for chemokine receptor CCR1. *Nat. Chem. Biol.* **18**, 264–271 (2022).
19. I. Masuho, S. Balaji, B. S. Muntean, N. K. Skamangas, S. Chavali, J. J. G. Tesmer, M. M. Babu, K. A. Martemyanov, A global map of G protein signaling regulation by RGS proteins. *Cell* **183**, 503–521.e19 (2020).
20. M. Abramow-Newerly, A. A. Roy, C. Nunn, P. Chidiac, RGS proteins have a signalling complex: Interactions between RGS proteins and GPCRs, effectors, and auxiliary proteins. *Cell. Signal.* **18**, 579–591 (2006).
21. J. Schwenk, M. Metz, G. Zolles, R. Turecek, T. Fritzius, W. Bildl, E. Tarusawa, A. Kulik, A. Unger, K. Ivankova, R. Seddik, J. Y. Tiao, M. Rajalu, J. Trojanova, V. Rohde, M. Gassmann, U. Schulte, B. Fakler, B. Bettler, Native $GABA_B$ receptors are heteromultimers with a family of auxiliary subunits. *Nature* **465**, 231–235 (2010).
22. S. Zheng, N. Abreu, J. Levitz, A. C. Kruse, Structural basis for KCTD-mediated rapid desensitization of $GABA_B$ signalling. *Nature* **567**, 127–131 (2019).
23. R. Turecek, J. Schwenk, T. Fritzius, K. Ivankova, G. Zolles, L. Adelfinger, V. Jacquier, V. Besseyrias, M. Gassmann, U. Schulte, B. Fakler, B. Bettler, Auxiliary $GABA_B$ receptor subunits uncouple G protein βγ subunits from effector channels to induce desensitization. *Neuron* **82**, 1032–1044 (2014).
24. A. Raveh, A. Cooper, L. Guy-David, E. Reuveny, Nonenzymatic rapid control of GIRK channel function by a G protein-coupled receptor kinase. *Cell* **143**, 750–760 (2010).
25. N. Abreu, A. Acosta-Ruiz, G. Xiang, J. Levitz, Mechanisms of differential desensitization of metabotropic glutamate receptors. *Cell Rep.* **35**, 109050 (2021).
26. V. Wolters, C. Krasel, J. Brockmann, M. Bunemann, Influence of gαq on the dynamics of m3-acetylcholine receptor-g-protein-coupled receptor kinase 2 interaction. *Mol. Pharmacol.* **87**, 9–17 (2015).
27. M. Stoeber, D. Jullié, J. Li, S. Chakraborty, S. Majumdar, N. A. Lambert, A. Manglik, M. von Zastrow, Agonist-selective recruitment of engineered protein probes and of GRK2 by opioid receptors in living cells. *eLife* **9**, e54208 (2020).
28. C. V. Carman, J. L. Parent, P. W. Day, A. N. Pronin, P. M. Sternweis, P. B. Wedegaertner, A. G. Gilman, J. L. Benovic, T. Kozasa, Selective regulation of $G\alpha_{q/11}$ by an RGS domain in the G protein-coupled receptor kinase, GRK2. *J. Biol. Chem.* **274**, 34483–34492 (1999).
29. P. W. Day, C. V. Carman, R. Sterne-Marr, J. L. Benovic, P. B. Wedegaertner, Differential interaction of GRK2 with members of the Gα q family. *Biochemistry* **42**, 9176–9184 (2003).
30. P. W. Day, J. J. G. Tesmer, R. Sterne-Marr, L. C. Freeman, J. L. Benovic, P. B. Wedegaertner, Characterization of the GRK2 binding site of $G\alpha_q$. *J. Biol. Chem.* **279**, 53643–53652 (2004).
31. V. M. Tesmer, T. Kawano, A. Shankaranarayanan, T. Kozasa, J. J. Tesmer, Snapshot of activated G proteins at the membrane: The $G\alpha_q$-GRK2-Gβγ complex. *Science* **310**, 1686–1690 (2005).
32. M. Sallese, S. Mariggiò, E. D'Urbano, A. Iacovelli, A. De Blasi, Selective regulation of Gq signaling by G protein-coupled receptor kinase 2: Direct interaction of kinase N terminus with activated Gαq. *Mol. Pharmacol.* **57**, 826–831 (2000).
33. H. Usui, M. Nishiyama, K. Moroi, T. Shibasaki, J. Zhou, J. Ishida, A. Fukamizu, T. Haga, S. Sekiya, S. Kimura, RGS domain in the amino-terminus of G protein-coupled receptor kinase 2 inhibits Gq-mediated signaling. *Int. J. Mol. Med.* **5**, 335–340 (2000).
34. R. Sterne-Marr, J. J. G. Tesmer, P. W. Day, R. A. P. Stracquatanio, J.-A. E. Cilente, K. E. O'Connor, A. N. Pronin, J. L. Benovic, P. B. Wedegaertner, G protein-coupled receptor kinase 2/$G\alpha_{q/11}$ interaction. A novel surface on a regulator of G protein signaling homology domain for binding Gα subunits. *J. Biol. Chem.* **278**, 6050–6058 (2003).
35. J. D. Sherrill, W. E. Miller, G protein-coupled receptor (GPCR) kinase 2 regulates agonist-independent $G_{q/11}$ signaling from the mouse cytomegalovirus GPCR M33. *J. Biol. Chem.* **281**, 39796–39805 (2006).
36. J. M. Willets, S. R. Nahorski, R. A. Challiss, Roles of phosphorylation-dependent and -independent mechanisms in the regulation of M1 muscarinic acetylcholine receptors by G protein-coupled receptor kinase 2 in hippocampal neurons. *J. Biol. Chem.* **280**, 18950–18958 (2005).
37. J. Luo, J. M. Busillo, J. L. Benovic, M3 muscarinic acetylcholine receptor-mediated signaling is regulated by distinct mechanisms. *Mol. Pharmacol.* **74**, 338–347 (2008).
38. G. K. Dhami, L. B. Dale, P. H. Anborgh, K. E. O'Connor-Halligan, R. Sterne-Marr, S. S. G. Ferguson, G Protein-coupled receptor kinase 2 regulator of G protein signaling homology domain binds to both metabotropic glutamate receptor 1a and $G\alpha_q$ to attenuate signaling. *J. Biol. Chem.* **279**, 16614–16620 (2004).
39. G. K. Dhami, P. H. Anborgh, L. B. Dale, R. Sterne-Marr, S. S. Ferguson, Phosphorylation-independent regulation of metabotropic glutamate receptor signaling by G protein-coupled receptor kinase 2. *J. Biol. Chem.* **277**, 25266–25272 (2002).
40. G. K. Dhami, A. V. Babwah, R. Sterne-Marr, S. S. Ferguson, Phosphorylation-independent regulation of metabotropic glutamate receptor 1 signaling requires g protein-coupled receptor kinase 2 binding to the second intracellular loop. *J. Biol. Chem.* **280**, 24420–24427 (2005).
41. F. M. Ribeiro, L. T. Ferreira, M. Paquet, T. Cregan, Q. Ding, R. Gros, S. S. G. Ferguson, Phosphorylation-independent regulation of metabotropic glutamate receptor 5 desensitization and internalization by G protein-coupled receptor kinase 2 in neurons. *J. Biol. Chem.* **284**, 23444–23453 (2009).
42. D. E. Clapham, Calcium signaling. *Cell* **131**, 1047–1058 (2007).
43. V. Dhyani, S. Gare, R. K. Gupta, S. Swain, K. V. Venkatesh, L. Giri, GPCR mediated control of calcium dynamics: A systems perspective. *Cell. Signal.* **74**, 109717 (2020).

44. A. Reiner, J. Levitz, Glutamatergic signaling in the central nervous system: Ionotropic and metabotropic receptors in concert. *Neuron* **98**, 1080–1098 (2018).
45. S. Kawabata, R. Tsutusmi, A. Kohara, T. Yamaguchi, S. Nakanishi, M. Okada, Control of calcium oscillations by phosphorylation of metabotropic glutamate receptors. *Nature* **383**, 89–92 (1996).
46. C. H. Kim, S. Braud, J. T. Isaac, K. W. Roche, Protein kinase C phosphorylation of the metabotropic glutamate receptor mGluR5 on Serine 839 regulates $Ca^{2+}$ oscillations. *J. Biol. Chem.* **280**, 25409–25415 (2005).
47. Y. Zhao, S. Araki, J. Wu, T. Teramoto, Y.-F. Chang, M. Nakano, A. S. Abdelfattah, M. Fujiwara, T. Ishihara, T. Nagai, R. E. Campbell, An expanded palette of genetically encoded $Ca^{2+}$ indicators. *Science* **333**, 1888–1891 (2011).
48. K. Hemstapat, T. de Paulis, Y. Chen, A. E. Brady, V. K. Grover, D. Alagille, G. D. Tamagnan, P. J. Conn, A novel class of positive allosteric modulators of metabotropic glutamate receptor subtype 1 interact with a site distinct from that of negative allosteric modulators. *Mol. Pharmacol.* **70**, 616–626 (2006).
49. A. L. Rodriguez, M. D. Grier, C. K. Jones, E. J. Herman, A. S. Kane, R. L. Smith, R. Williams, Y. Zhou, J. E. Marlo, E. L. Days, T. N. Blatt, S. Jadhav, U. N. Menon, P. N. Vinson, J. M. Rook, S. R. Stauffer, C. M. Niswender, C. W. Lindsley, C. D. Weaver, P. J. Conn, Discovery of novel allosteric modulators of metabotropic glutamate receptor subtype 5 reveals chemical and functional diversity and in vivo activity in rat behavioral models of anxiolytic and antipsychotic activity. *Mol. Pharmacol.* **78**, 1105–1123 (2010).
50. K. Kawakami, M. Yanagawa, S. Hiratsuka, M. Yoshida, Y. Ono, M. Hiroshima, M. Ueda, J. Aoki, Y. Sako, A. Inoue, Heterotrimeric Gq proteins act as a switch for GRK5/6 selectivity underlying β-arrestin transducer bias. *Nat. Commun.* **13**, 487 (2022).
51. J. de Juan-Sanz, G. T. Holt, E. R. Schreiter, F. de Juan, D. S. Kim, T. A. Ryan, Axonal endoplasmic reticulum $Ca^{2+}$ content controls release probability in CNS nerve terminals. *Neuron* **93**, 867–881.e6 (2017).
52. A. Acosta-Ruiz, V. A. Gutzeit, M. J. Skelly, S. Meadows, J. Lee, P. Parekh, A. G. Orr, C. Liston, K. E. Pleil, J. Broichhagen, J. Levitz, Branched photoswitchable tethered ligands enable ultra-efficient optical control and detection of G protein-coupled receptors in vivo. *Neuron* **105**, 446–463.e13 (2020).
53. S. A. Hires, Y. Zhu, R. Y. Tsien, Optical measurement of synaptic glutamate spillover and reuptake by linker optimized glutamate-sensitive fluorescent reporters. *Proc. Natl. Acad. Sci. U.S.A.* **105**, 4411–4416 (2008).
54. J. S. Marvin, B. G. Borghuis, L. Tian, J. Cichon, M. T. Harnett, J. Akerboom, A. Gordus, S. L. Renninger, T.-W. Chen, C. I. Bargmann, M. B. Orger, E. R. Schreiter, J. B. Demb, W.-B. Gan, S. A. Hires, L. L. Looger, An optimized fluorescent probe for visualizing glutamate neurotransmission. *Nat. Methods* **10**, 162–170 (2013).
55. V. A. Gutzeit, A. Acosta-Ruiz, H. Munguba, S. Häfner, A. Landra-Willm, B. Mathes, J. Mony, D. Yarotski, K. Börjesson, C. Liston, G. Sandoz, J. Levitz, J. Broichhagen, A fine-tuned azobenzene for enhanced photopharmacology in vivo. *Cell Chem. Biol.* **28**, 1648–1663. e16 (2021).
56. D. T. Lodowski, J. A. Pitcher, W. D. Capel, R. J. Lefkowitz, J. J. Tesmer, Keeping G proteins at bay: A complex between G protein-coupled receptor kinase 2 and Gβγ. *Science* **300**, 1256–1262 (2003).
57. D. M. Thal, R. Y. Yeow, C. Schoenau, J. Huber, J. J. Tesmer, Molecular mechanism of selectivity among G protein-coupled receptor kinase 2 inhibitors. *Mol. Pharmacol.* **80**, 294–303 (2011).
58. V. M. Tesmer, S. Lennarz, G. Mayer, J. J. Tesmer, Molecular mechanism for inhibition of g protein-coupled receptor kinase 2 by a selective RNA aptamer. *Structure* **20**, 1300–1309 (2012).
59. K. T. Homan, E. Wu, M. W. Wilson, P. Singh, S. D. Larsen, J. J. G. Tesmer, Structural and functional analysis of g protein-coupled receptor kinase inhibition by paroxetine and a rationally designed analog. *Mol. Pharmacol.* **85**, 237–248 (2014).
60. K. T. Homan, J. J. Tesmer, Molecular basis for small molecule inhibition of G protein-coupled receptor kinases. *ACS Chem. Biol.* **10**, 246–256 (2015).
61. H. V. Waldschmidt, K. T. Homan, O. Cruz-Rodríguez, M. C. Cato, J. Waninger-Saroni, K. M. Larimore, A. Cannavo, J. Song, J. Y. Cheung, P. D. Kirchhoff, W. J. Koch, J. J. G. Tesmer, S. D. Larsen, Structure-based design, synthesis, and biological evaluation of highly selective and potent G protein-coupled receptor kinase 2 inhibitors. *J. Med. Chem.* **59**, 3793–3807 (2016).
62. H. V. Waldschmidt, K. T. Homan, M. C. Cato, O. Cruz-Rodríguez, A. Cannavo, M. W. Wilson, J. Song, J. Y. Cheung, W. J. Koch, J. J. G. Tesmer, S. D. Larsen, Structure-based design of highly selective and potent G protein-coupled receptor kinase 2 inhibitors based on paroxetine. *J. Med. Chem.* **60**, 3052–3069 (2017).
63. C. V. Carman, L. S. Barak, C. Chen, L. Y. Liu-Chen, J. J. Onorato, S. P. Kennedy, M. G. Caron, J. L. Benovic, Mutational analysis of Gβγ and phospholipid interaction with G protein-coupled receptor kinase 2. *J. Biol. Chem.* **275**, 10443–10452 (2000).
64. G. Kong, R. Penn, J. L. Benovic, A β-adrenergic receptor kinase dominant negative mutant attenuates desensitization of the β 2-adrenergic receptor. *J. Biol. Chem.* **269**, 13084–13087 (1994).
65. G. L. Waldo, T. K. Ricks, S. N. Hicks, M. L. Cheever, T. Kawano, K. Tsuboi, X. Wang, C. Montell, T. Kozasa, J. Sondek, T. K. Harden, Kinetic scaffolding mediated by a phospholipase C-β and Gq signaling complex. *Science* **330**, 974–980 (2010).
66. A. M. Lyon, S. Dutta, C. A. Boguth, G. Skiniotis, J. J. Tesmer, Full-length $G\alpha_q$-phospholipase C-β3 structure reveals interfaces of the C-terminal coiled-coil domain. *Nat. Struct. Mol. Biol.* **20**, 355–362 (2013).
67. A. M. Lyon, V. M. Tesmer, V. D. Dhamsania, D. M. Thal, J. Gutierrez, S. Chowdhury, K. C. Suddala, J. K. Northup, J. J. G. Tesmer, An autoinhibitory helix in the C-terminal region of phospholipase C-β mediates Galphaq activation. *Nat. Struct. Mol. Biol.* **18**, 999–1005 (2011).
68. A. Shankaranarayanan, D. M. Thal, V. M. Tesmer, D. L. Roman, R. R. Neubig, T. Kozasa, J. J. G. Tesmer, Assembly of high order $G\alpha_q$-effector complexes with RGS proteins. *J. Biol. Chem.* **283**, 34923–34934 (2008).
69. J. Inglese, W. J. Koch, M. G. Caron, R. J. Lefkowitz, Isoprenylation in regulation of signal transduction by G-protein-coupled receptor kinases. *Nature* **359**, 147–150 (1992).
70. H. Dana, B. Mohar, Y. Sun, S. Narayan, A. Gordus, J. P. Hasseman, G. Tsegaye, G. T. Holt, A. Hu, D. Walpita, R. Patel, J. J. Macklin, C. I. Bargmann, M. B. Ahrens, E. R. Schreiter, V. Jayaraman, L. L. Looger, K. Svoboda, D. S. Kim, Sensitive red protein calcium indicators for imaging neural activity. *eLife* **5**, e12727 (2016).
71. J. B. Schachter, S. M. Sromek, R. A. Nicholas, T. K. Harden, HEK293 human embryonic kidney cells endogenously express the P2Y1 and P2Y2 receptors. *Neuropharmacology* **36**, 1181–1187 (1997).
72. B. K. Atwood, J. Lopez, J. Wager-Miller, K. Mackie, A. Straiker, Expression of G protein-coupled receptors and related proteins in HEK293, AtT20, BV2, and N18 cell lines as revealed by microarray analysis. *BMC Genomics* **12**, 14 (2011).
73. S. Rajagopal, J. Kim, S. Ahn, S. Craig, C. M. Lam, N. P. Gerard, C. Gerard, R. J. Lefkowitz, β-arrestin- but not G protein-mediated signaling by the "decoy" receptor CXCR7. *Proc. Natl. Acad. Sci. U.S.A.* **107**, 628–632 (2010).
74. S. Pandey, P. Kumari, M. Baidya, R. Kise, Y. Cao, H. Dwivedi-Agnihotri, R. Banerjee, X. X. Li, C. S. Cui, J. D. Lee, K. Kawakami, J. Maharana, A. Ranjan, M. Chaturvedi, G. D. Jhingan, S. A. Laporte, T. M. Woodruff, A. Inoue, A. K. Shukla, Intrinsic bias at non-canonical, β-arrestin-coupled seven transmembrane receptors. *Mol. Cell* **81**, 4605–4621.e11 (2021).
75. T. Flock, A. S. Hauser, N. Lund, D. E. Gloriam, S. Balaji, M. M. Babu, Selectivity determinants of GPCR-G-protein binding. *Nature* **545**, 317–322 (2017).
76. I. J. Fisher, M. L. Jenkins, G. G. Tall, J. E. Burke, A. V. Smrcka, Activation of phospholipase C β by Gβγ and $G\alpha_q$ involves C-terminal rearrangement to release autoinhibition. *Structure* **28**, 810–819.e5 (2020).
77. P. Gerwins, B. B. Fredholm, Stimulation of adenosine A1 receptors and bradykinin receptors, which act via different G proteins, synergistically raises inositol 1,4,5-trisphosphate and intracellular free calcium in DDT1 MF-2 smooth muscle cells. *Proc. Natl. Acad. Sci. U.S.A.* **89**, 7330–7334 (1992).
78. F. Okajima, Y. Kondo, Synergism in cytosolic $Ca^{2+}$ mobilization between bradykinin and agonists for pertussis toxin-sensitive G-protein-coupled receptors in NG 108-15 cells. *FEBS Lett.* **301**, 223–226 (1992).
79. K. A. Buckley, S. C. Wagstaff, G. McKay, A. Gaw, R. A. Hipskind, G. Bilbe, J. A. Gallagher, W. B. Bowler, Parathyroid hormone potentiates nucleotide-induced $Ca^{2+}$ i release in rat osteoblasts independently of Gq activation or cyclic monophosphate accumulation. A mechanism for localizing systemic responses in bone. *J. Biol. Chem.* **276**, 9565–9571 (2001).
80. E. Doumazane, P. Scholler, J. M. Zwier, E. Trinquet, P. Rondard, J.-P. Pin, A new approach to analyze cell surface protein complexes reveals specific heterodimeric metabotropic glutamate receptors. *FASEB J.* **25**, 66–77 (2011).
81. A. Qifti, L. Jackson, A. Singla, O. Garwain, S. Scarlata, Stimulation of phospholipase Cβ1 by $G\alpha_q$ promotes the assembly of stress granule proteins. *Sci. Signal.* **14**, eaav1012 (2021).
82. C. D. Van Raamsdonk, V. Bezrookove, G. Green, J. Bauer, L. Gaugler, J. M. O'Brien, E. M. Simpson, G. S. Barsh, B. C. Bastian, Frequent somatic mutations of GNAQ in uveal melanoma and blue naevi. *Nature* **457**, 599–602 (2009).
83. N. Arang, J. S. Gutkind, G protein-coupled receptors and heterotrimeric G proteins as cancer drivers. *FEBS Lett.* **594**, 4201–4232 (2020).
84. E. Kostenis, E. M. Pfeil, S. Annala, Heterotrimeric $G_q$ proteins as therapeutic targets? *J. Biol. Chem.* **295**, 5206–5215 (2020).
85. J. Wang, C. Gareri, H. A. Rockman, G-protein-coupled receptors in heart disease. *Circ. Res.* **123**, 716–735 (2018).
86. P. Chidiac, E. M. Ross, Phospholipase C-β1 directly accelerates GTP hydrolysis by $G\alpha_q$ and acceleration is inhibited by Gβ γ subunits. *J. Biol. Chem.* **274**, 19639–19643 (1999).
87. E. S. F. Matthees, R. S. Haider, C. Hoffmann, J. Drube, Differential regulation of GPCRs-are GRK expression levels the key? *Front. Cell Dev. Biol.* **9**, 687489 (2021).
88. S. M. Schumacher, E. Gao, M. Cohen, M. Lieu, J. K. Chuprun, W. J. Koch, A peptide of the RGS domain of GRK2 binds and inhibits $G\alpha_q$ to suppress pathological cardiac hypertrophy and dysfunction. *Sci. Signal.* **9**, ra30 (2016).
89. J. Nagai, A. Bellafard, Z. Qu, X. Yu, M. Ollivier, M. R. Gangwani, B. Diaz-Castro, G. Coppola, S. M. Schumacher, P. Golshani, V. Gradinaru, B. S. Khakh, Specific and behaviorally

consequential astrocyte $G_q$ GPCR signaling attenuation in vivo with iβARK. *Neuron* **109**, 2256–2274.e9 (2021).
90. D. Kankanamge, S. Ubeysinghe, M. Tennakoon, P. D. Pantula, K. Mitra, L. Giri, A. Karunarathne, Dissociation of the G protein βγ from the Gq-PLCβ complex partially attenuates PIP2 hydrolysis. *J. Biol. Chem.* **296**, 100702 (2021).
91. C. A. Durkee, A. Covelo, J. Lines, P. Kofuji, J. Aguilar, A. Araque, $G_{i/o}$ protein-coupled receptors inhibit neurons but activate astrocytes and stimulate gliotransmission. *Glia* **67**, 1076–1093 (2019).
92. V. Kellner, C. J. Kersbergen, S. Li, T. A. Babola, G. Saher, D. E. Bergles, Dual metabotropic glutamate receptor signaling enables coordination of astrocyte and neuron activity in developing sensory domains. *Neuron* **109**, 2545–2555.e7 (2021).
93. A. I. Jiménez, E. Castro, M. Mirabet, R. Franco, E. G. Delicado, M. T. Miras-Portugal, Potentiation of ATP calcium responses by A2B receptor stimulation and other signals coupled to Gs proteins in type-1 cerebellar astrocytes. *Glia* **26**, 119–128 (1999).
94. I. Gomes, M. A. Ayoub, W. Fujita, W. C. Jaeger, K. D. G. Pfleger, L. A. Devi, G protein-coupled receptor heteromers. *Annu. Rev. Pharmacol. Toxicol.* **56**, 403–425 (2016).
95. I. Sebastianutto, E. Goyet, L. Andreoli, J. Font-Ingles, D. Moreno-Delgado, N. Bouquier, C. Jahannault-Talignani, E. Moutin, L. D. Menna, N. Maslava, J.-P. Pin, L. Fagni, F. Nicoletti, F. Ango, M. A. Cenci, J. Perroy, D1-mGlu5 heteromers mediate noncanonical dopamine signaling in Parkinson's disease. *J. Clin. Invest.* **130**, 1168–1184 (2020).
96. V. Chua, D. Lapadula, C. Randolph, J. L. Benovic, P. B. Wedegaertner, A. E. Aplin, Dysregulated GPCR signaling and therapeutic options in uveal melanoma. *Mol. Cancer Res.* **15**, 501–506 (2017).
97. M. Maziarz, J.-C. Park, A. Leyme, A. Marivin, A. Garcia-Lopez, P. P. Patel, M. Garcia-Marcos, Revealing the activity of trimeric G-proteins in live cells with a versatile biosensor design. *Cell* **182**, 770–785.e16 (2020).
98. J. A. Pitcher, J. Inglese, J. B. Higgins, J. L. Arriza, P. J. Casey, C. Kim, J. L. Benovic, M. M. Kwatra, M. G. Caron, R. J. Lefkowitz, Role of βγ subunits of G proteins in targeting the β-adrenergic receptor kinase to membrane-bound receptors. *Science* **257**, 1264–1267 (1992).
99. T. Sungkaworn, M.-L. Jobin, K. Burnecki, A. Weron, M. J. Lohse, D. Calebiro, Single-molecule imaging reveals receptor-G protein interactions at cell surface hot spots. *Nature* **550**, 543–547 (2017).
100. C. Ribas, P. Penela, C. Murga, A. Salcedo, C. García-Hoz, M. Jurado-Pueyo, I. Aymerich, F. M. Jr., The G protein-coupled receptor kinase (GRK) interactome: Role of GRKs in GPCR regulation and signaling. *Biochim. Biophys. Acta* **1768**, 913–922 (2007).
101. S. M. Sulon, J. L. Benovic, Targeting G protein-coupled receptor kinases (GRKs) to G protein-coupled receptors. *Curr. Opin. Endocr. Metab. Res.* **16**, 56–65 (2021).
102. J. Morstein, G. Romano, B. E. Hetzler, A. Plante, C. Haake, J. Levitz, D. Trauner, Photoswitchable serotonins for optical control of the 5-HT2A receptor. *Angew. Chem. Int. Ed. Engl.* **61**, e202117094 (2022).
103. M. Vivaudou, K. W. Chan, J. L. Sui, L. Y. Jan, E. Reuveny, D. E. Logothetis, Probing the G-protein regulation of GIRK1 and $GIRK_4$, the two subunits of the KACh channel, using functional homomeric mutants. *J. Biol. Chem.* **272**, 31553–31560 (1997).
104. V. A. Gutzeit, J. Thibado, D. S. Stor, Z. Zhou, S. C. Blanchard, O. S. Andersen, J. Levitz, Conformational dynamics between transmembrane domains and allosteric modulation of a metabotropic glutamate receptor. *eLife* **8**, e45116 (2019).

**Acknowledgments:** We thank the Levitz and Lee laboratories for technical support and helpful discussions. **Funding:** This work was supported by National Institutes of Health grant R35GM124731 (J.L.); Rohr Family Research Scholar Award (J.L.); Monique Weill-Caulier Award (J.L.); Swiss National Science Foundation Fellowship PCEFP3_181282 (M.S.); Pritzker Neuropsychiatric Disorders Research Consortium (F.S.L.); NIH grant R01NS116747 (J.S.D.); Japan Society for the Promotion of Science KAKENHI grants 21H04791, 21H05113, JPJSBP120213501, and JPJSBP120218801 (A.I.); Japan Science and Technology Agency (A.I. ); FOREST Program JPMJFR215T (A.I.); the Uehara Memorial Foundation (A.I.); and Daiichi Sankyo Foundation of Life Science (A.I.). **Author contributions:** Conceptualization: G.X., A.A.-R., M.S., J.S.D., and J.L. Methodology: G.X., A.A.-R., J.B., A.I., M.S., J.S.D., and J.L. Investigation: G.X., A.A.-R., A.R.-M., M.K., J.K., and J.D.M. Supervision: M.S., F.S.L., and J.L. Writing—original draft: J.L. Writing—review and editing: G.X., A.A.-R., A.R.-M., M.K., J.K., J.D.M., J.B., A.I., F.S.L., M.S., J.S.D., and J.L. **Competing interests:** The authors declare that they have no competing interests. **Data and materials availability:** All data needed to evaluate the conclusions in the paper are present in the paper and/or the Supplementary Materials. All materials can be provided pending a completed material transfer agreement. Requests for the GRK2/3 KO cell line should be submitted to iaska@tohoko.ac.jp. Requests for all other materials should be submitted to jtl2003@med.cornell.edu.

Submitted 1 April 2022
Accepted 6 October 2022
Published 25 November 2022
10.1126/sciadv.abq3363

ScienceAdvances

# Control of G#$_q$ signaling dynamics and GPCR cross-talk by GRKs

Guoqing XiangAmanda Acosta-RuizArthur Radoux-MergaultMelanie KristtJihye KimJared D. MoonJohannes BroichhagenAsuka InoueFrancis S. LeeMiriam StoeberJeremy S. DittmanJoshua Levitz

*Sci. Adv.*, 8 (47), eabq3363. • DOI: 10.1126/sciadv.abq3363